OTULIN Prevents Liver Inflammation and Hepatocellular Carcinoma by Inhibiting FADD- and RIPK1 Kinase-Mediated Hepatocyte Apoptosis

Verboom, Lien; Martens, Arne; Priem, Dario; Hoste, Esther; Sze, Mozes; Vikkula, Hanna; Van Hove, Lisette; Voet, Sofie; Roels, Jana; Maelfait, Jonathan

Published in:
Cell reports

DOI:
10.1016/j.celrep.2020.01.028

Publication date:
2020

Article

Cell Reports

OTULIN Prevents Liver Inflammation and Hepatocellular Carcinoma by Inhibiting FADD- and RIPK1 Kinase-Mediated Hepatocyte Apoptosis

Graphical Abstract

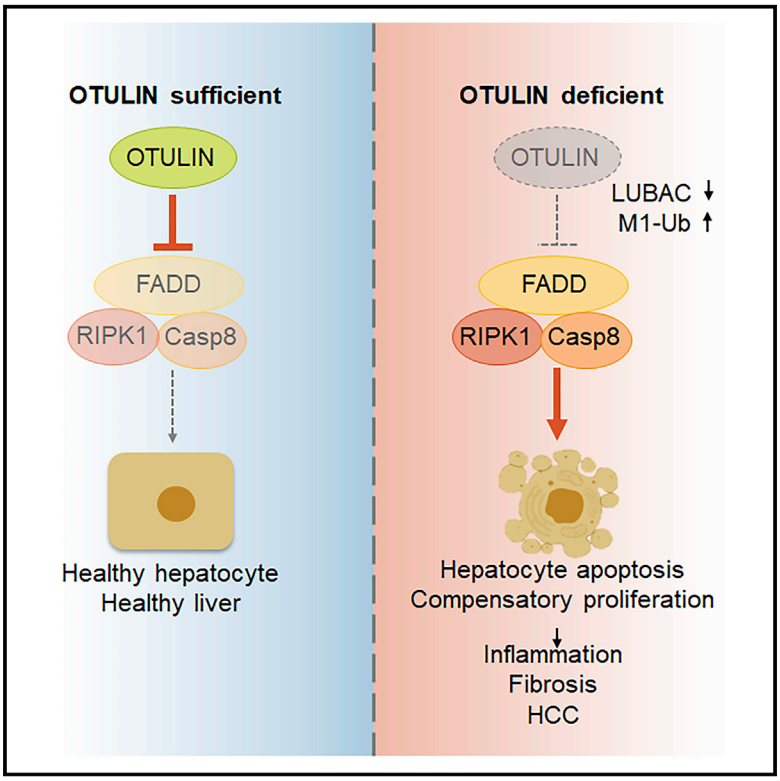

Highlights

- OTULIN is a crucial hepatoprotective factor
- OTULIN prevents chronic liver inflammation, fibrosis, and liver cancer
- OTULIN protects hepatocytes from FADD and RIPK1-dependent apoptosis
- Type I interferon signaling contributes to liver pathology in OTULIN-deficient mice

Authors

Lien Verboom, Arne Martens, Dario Priem, ..., Manolis Pasparakis, Mathieu J.M. Bertrand, Geert van Loo

Correspondence

geert.vanloo@irc.vib-ugent.be

In Brief

Hepatocellular carcinoma (HCC) develops as a result of chronic liver inflammation. Verboom et al. identify OTULIN as a critical liver-protective protein, essential in preventing hepatocyte apoptosis, which could trigger compensatory hepatocyte proliferation, chronic liver inflammation, fibrosis, and HCC.

Verboom et al., 2020, Cell Reports *30*, 2237–2247
February 18, 2020
https://doi.org/10.1016/j.celrep.2020.01.028

CellPress

Cell Reports
Article

OTULIN Prevents Liver Inflammation and Hepatocellular Carcinoma by Inhibiting FADD- and RIPK1 Kinase-Mediated Hepatocyte Apoptosis

Lien Verboom,[1,2] Arne Martens,[1,2] Dario Priem,[1,2] Esther Hoste,[1,2] Mozes Sze,[1,2] Hanna Vikkula,[1,2] Lisette Van Hove,[1,2] Sofie Voet,[1,2] Jana Roels,[1,3] Jonathan Maelfait,[1,2] Laura Bongiovanni,[4,5] Alain de Bruin,[4,5] Charlotte L. Scott,[1,2] Yvan Saeys,[1,3] Manolis Pasparakis,[6,7] Mathieu J.M. Bertrand,[1,2] and Geert van Loo[1,2,8,*]

[1]VIB Center for Inflammation Research, 9052 Ghent, Belgium
[2]Department of Biomedical Molecular Biology, Ghent University, 9052 Ghent, Belgium
[3]Department of Applied Mathematics, Computer Sciences, and Statistics, Ghent University, 9052 Ghent, Belgium
[4]Dutch Molecular Pathology Center, Department of Pathobiology, Faculty of Veterinary Medicine, Utrecht University, Utrecht 3584, the Netherlands
[5]Department of Pediatrics, University Medical Center Groningen, University of Groningen, Groningen 9713, the Netherlands
[6]Institute for Genetics, Centre for Molecular Medicine (CMMC), University of Cologne, 50931 Cologne, Germany
[7]Cologne Excellence Cluster on Cellular Stress Responses in Aging-Associated Diseases (CECAD), University of Cologne, 50931 Cologne, Germany
[8]Lead Contact
*Correspondence: geert.vanloo@irc.vib-ugent.be
https://doi.org/10.1016/j.celrep.2020.01.028

SUMMARY

Inflammatory signaling pathways are tightly regulated to avoid chronic inflammation and the development of disease. OTULIN is a deubiquitinating enzyme that controls inflammation by cleaving linear ubiquitin chains generated by the linear ubiquitin chain assembly complex. Here, we show that ablation of OTULIN in liver parenchymal cells in mice causes severe liver disease which is characterized by liver inflammation, hepatocyte apoptosis, and compensatory hepatocyte proliferation, leading to steatohepatitis, fibrosis, and hepatocellular carcinoma (HCC). Genetic ablation of Fas-associated death domain (FADD) completely rescues and knockin expression of kinase inactive receptor-interacting protein kinase 1 (RIPK1) significantly protects mice from developing liver disease, demonstrating that apoptosis of OTULIN-deficient hepatocytes triggers disease pathogenesis in this model. Finally, we demonstrate that type I interferons contribute to disease in hepatocyte-specific OTULIN-deficient mice. Our study reveals the critical importance of OTULIN in protecting hepatocytes from death, thereby preventing the development of chronic liver inflammation and HCC.

INTRODUCTION

Liver cancer is the second most frequent cause of cancer-related deaths and the fifth most common type of cancer worldwide (Ringelhan et al., 2018). Of all of the primary liver cancers, hepatocellular carcinoma (HCC) is the most frequent, responsible for 80%–90% of all cases, and nearly all develop as a result of chronic liver inflammation, inducing fibrosis, cirrhosis, and finally HCC. There is clear evidence that cell death represents a basic biological process in liver cancer, wherein hepatocyte death induces compensatory hepatocyte regeneration, chronic liver inflammation, and activation of non-parenchymal cells, promoting liver fibrosis and tumorigenesis (Luedde and Schwabe, 2011; Kondylis and Pasparakis, 2019).

Tumor necrosis factor (TNF) is a major inflammatory cytokine, capable of inducing inflammatory gene expression, but also of triggering cell death. Many studies have shown that optimal regulation of TNF signaling is essential to maintain liver homeostasis and prevent liver inflammation and inflammation-induced HCC (Luedde et al., 2014). Inflammatory signaling, such as by TNF, is heavily controlled by ubiquitination, a posttranslational modification of proteins (Iwai et al., 2014). Sensing of TNF by TNF receptor 1 (TNFR1) initiates the assembly of a receptor-proximal complex, known as complex I, which activates the mitogen-activated protein kinase (MAPK) and nuclear factor-κB (NF-κB) signaling pathways (Ting and Bertrand, 2016). The initial binding of TNFR1-associated death domain protein (TRADD) and receptor-interacting protein kinase 1 (RIPK1) to the receptor allows the subsequent recruitment of TNF receptor-associated factor 2 (TRAF2) and of the E3 ubiquitin ligases cellular inhibitors of apoptosis 1 and 2 (cIAP1/2). The K63-ubiquitin chains generated by cIAP1/2 serve as docking stations for the adaptor proteins TAB2/3 and for the recruitment of the kinase TAK1, which subsequently activate the MAPK signaling pathways. These K63-ubiquitin chains also assist in recruiting the linear ubiquitin chain assembly complex (LUBAC, composed of HOIL-1, HOIP, and SHARPIN), which further conjugates complex I components with linear-ubiquitin chains. The adaptor protein NEMO binds to these linear chains and brings the kinases IKKα and IKKβ to the complex, thereby allowing activation of the NF-κB pathway. NEMO recruitment to the complex also

enables activation of the kinases TBK1/IKKε, which may regulate NF-κB activation (Clark et al., 2011; Lafont et al., 2018; Xu et al., 2018). Upon activation, the MAPK and NF-κB pathways drive the expression of a large set of genes, including pro-inflammatory genes (Ting and Bertrand, 2016).

The linear-ubiquitin chains generated by the LUBAC in the TNFR1 pathway are therefore essential for the NF-κB-dependent expression of pro-inflammatory genes, but they were also shown to play a double and crucial role in preventing TNF cytotoxicity. Apart from pro-inflammatory molecules, the activation of NF-κB also leads to the transcriptional upregulation of anti-apoptotic proteins, which protect cells from RIPK1 kinase-independent apoptosis (Wang et al., 2008). In addition, the linear ubiquitin-dependent phosphorylation of RIPK1 by IKKα/β and TBK1/IKKε was shown to protect cells from RIPK1 kinase-dependent apoptosis (Dondelinger et al., 2015, 2019; Lafont et al., 2018; Xu et al., 2018; Ting and Bertrand, 2016). Consequently, when these protective brakes are compromised, such as following LUBAC deficiency (Peltzer et al., 2014, 2018; Priem et al., 2019), activated TRADD and RIPK1 dissociate from complex I, and respectively induce RIPK1 kinase-independent and -dependent apoptotic cascades through association with Fas-associated death domain (FADD) protein and procaspase-8 to form the cytosolic death-inducing complex II. Necroptosis occurs when caspase-8 activation is blocked and involves RIPK1 kinase-dependent recruitment of RIPK3 and mixed-lineage kinase domain-like protein (MLKL) to complex II, inducing strong inflammatory responses (Ting and Bertrand, 2016). Hence, LUBAC activity is essential in preventing apoptotic and necroptotic cell death, and HOIP- and HOIL-1-deficient mice die during development (Peltzer et al., 2014, 2018).

Ubiquitination is a reversible process, and the deubiquitinating (DUB) enzyme OTULIN (OTU deubiquitinase with linear linkage specificity, also known as Fam105b or Gumby) exclusively cleaves the linear ubiquitin chains generated by LUBAC, and hence critically controls inflammatory and cell death responses (Keusekotten et al., 2013; Rivkin et al., 2013). Accordingly, mice harboring a point mutation abolishing the ability of OTULIN to bind ubiquitin ("Gumby" mice) or knockin mice expressing a catalytically inactive variant of OTULIN die *in utero* due to excessive inflammatory cell death (Rivkin et al., 2013; Heger et al., 2018). However, mice with inducible OTULIN deficiency were shown to be viable and develop a severe inflammatory disease (Damgaard et al., 2016), resembling an autoinflammatory syndrome in humans carrying homozygous hypomorphic OTULIN mutations, called OTULIN-related autoinflammatory syndrome (ORAS, also known as otulipenia) (Zhou et al., 2016; Damgaard et al., 2016, 2019; Nabavi et al., 2019). Although OTULIN was originally shown to negatively regulate LUBAC activity, its deficiency does not induce LUBAC hyperactivity, as expected, but rather suppresses its function. OTULIN-, HOIP-, and HOIL-1-deficient mice have very similar phenotypes displaying embryonic lethality due to uncontrolled cell death. Together, these data showed that OTULIN promotes rather than counteracts LUBAC signaling by preventing LUBAC autoubiquitination through the removal of linear ubiquitin chains from LUBAC (Heger et al., 2018).

In light of the reported function of OTULIN in regulating both TNF-induced NF-κB signaling and cell death (Keusekotten et al., 2013; Damgaard et al., 2016, 2019; Heger et al., 2018), we questioned the role of OTULIN in liver (patho)physiology. For this, we generated OTULIN conditional knockout (KO) mice that are specifically deficient for OTULIN in liver parenchymal cells. These mice spontaneously develop chronic liver inflammation, fibrosis, and HCCs, illustrating the importance of OTULIN in normal liver tissue homeostasis. Chronic liver pathology results from the hypersensitivity of OTULIN-deficient hepatocytes to spontaneous FADD- and RIPK1 kinase activity-dependent apoptosis, which triggers compensatory hepatocyte proliferation and inflammation. Type I interferon (IFN) signaling also contributes to liver pathology in OTULIN-deficient mice. Together, these studies establish OTULIN as a crucial hepatoprotective factor.

RESULTS

Development of a Severe Liver Pathology in Hepatocyte-Specific OTULIN KO Mice

Otulin-targeted ES cells (*Otulin*$^{tm1a(EUCOMM)Hmgu}$) were used to generate chimeric mice that transmitted the targeted allele to their offspring. Mice homozygous for the LoxP-flanked *Otulin* allele (*Otulin*$^{FL/FL}$) express normal levels of OTULIN and develop normally (data not shown). Deletion of the LoxP-flanked *Otulin* alleles through the expression of a ubiquitously expressed Cre recombinase leads to a loss of OTULIN protein, as shown in mouse embryonic fibroblasts (MEFs) (Figure S1A). In agreement with previous studies (Rivkin et al., 2013; Damgaard et al., 2016; Heger et al., 2018), full-body OTULIN KO mice are not viable (Figure S1B), preventing further study. To study the role of OTULIN in hepatocytes and in liver physiology and pathology, we crossed the *Otulin*$^{FL/FL}$ mice with a transgenic mouse line that expresses Cre under the control of the liver-specific albumin/α-fetoprotein (AFP) promoter/enhancer (Alfp-Cre), which mediates efficient Cre recombination in liver parenchymal cells (Kellendonk et al., 2000; Figures S1C and S1D). Hepatocyte-specific OTULIN KO (*Otulin*$^{FL/FL}$/Alfp-Cre, liver parenchymal cell-specific OTULIN KO [OTULIN^{LPC-KO}]) mice were born with normal Mendelian segregation. Immunoblot analysis of liver protein extracts revealed efficient ablation of OTULIN in the livers of OTULIN^{LPC-KO} mice (Figure 1A). Residual OTULIN expression in these livers can be attributed to nonparenchymal liver cells that are not targeted by the Alfp-Cre allele.

The dissection of livers from 8- to 10-week-old OTULIN^{LPC-KO} mice revealed the presence of a severe liver phenotype. All OTULIN^{LPC-KO} livers displayed hepatomegaly and an aberrant liver architecture with the presence of numerous small but macroscopically visible nodules, in contrast to littermate control mice that did not show any overt liver pathology (Figures 1B, S2A, and S2B). At the same time, OTULIN^{LPC-KO} mice displayed elevated levels of the liver-specific enzymes aspartate transaminase (AST), alanine transaminase (ALT), and alkaline phosphatase (ALP), indicative of liver damage (Figure 1C), and also displayed hyperbilirubinemia, indicative of cholestasis (Figure 1C). Histological analysis confirmed a severe chronic inflammatory liver disease characterized by immune cell infiltration,

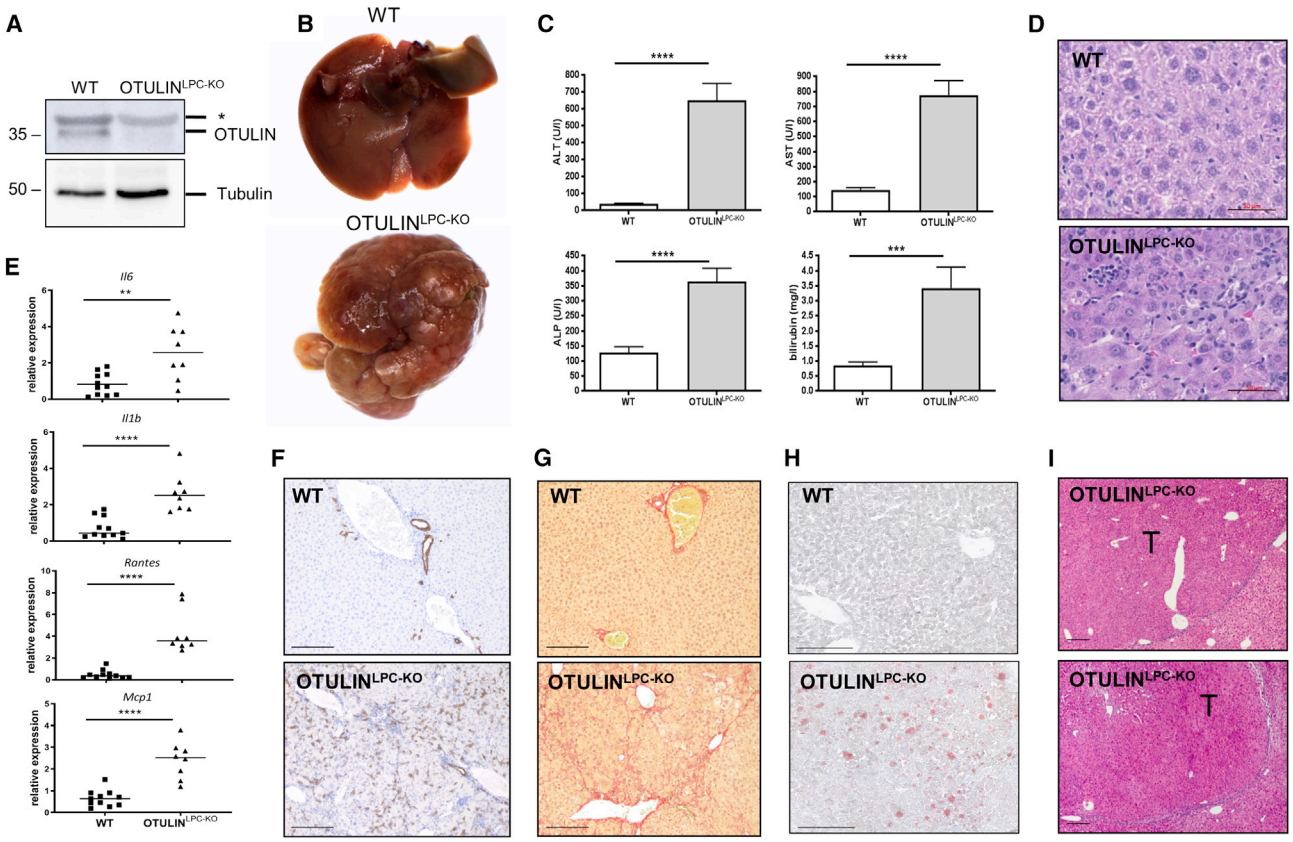

Figure 1. Development of a Severe Liver Phenotype in OTULIN^{LPC-KO} Mice

(A) Western blot analysis for OTULIN expression in total liver lysates from a control wild-type (WT) and OTULIN^{LPC-KO} littermate mouse. Anti-tubulin immunoblotting was used as loading control. *, unspecific. Data are representative of three independent experiments.

(B) Macroscopic pictures of representative livers from a 10-week-old WT and OTULIN^{LPC-KO} littermate mouse.

(C) Serum ALT, AST, ALP, and bilirubin levels of control (WT; n = 11) and OTULIN^{LPC-KO} (n = 7) mice. Data are presented as mean ± SEM. ***p < 0.001; ****p < 0.0001.

(D) Representative H&E-stained liver section from 10-week-old WT and OTULIN^{LPC-KO} mice demonstrating the loss of normal hepatic architecture and multifocal, lobular infiltration of mononuclear cells in the livers of OTULIN^{LPC-KO} mice. Scale bar, 50 μm.

(E) Relative mRNA levels of *Il6*, *Il1β*, *Mcp1*, and *Rantes* in total liver lysates from 10-week-old OTULIN^{LPC-KO} mice (n = 8) and control (WT, n = 11) mice. Data are presented as mean ± SEM. **p < 0.01; ***p < 0.001; ****p < 0.0001.

(F and G) Cytokeratin 19 (CK19) (F) and Sirius Red (G) staining on liver sections from 10-week-old WT and OTULIN^{LPC-KO} mice demonstrating oval cell hyperplasia and fibrosis in OTULIN^{LPC-KO} livers. Scale bar, 200 μm.

(H) Representative oil red O-stained liver cryosections from 10-week-old WT and OTULIN^{LPC-KO} mice. Scale bar, 200 μm.

(I) Representative H&E-stained liver section showing early well-differentiated HCC in 6-month-old OTULIN^{LPC-KO} mice. T, tumor. Scale bar, 200 μm.

proliferation of oval cells, and hypertrophy of hepatocytes (Figures S2C–S2H). In addition, the OTULIN-deficient livers demonstrated multifocal cell death of individual hepatocytes and an increase in the number of mitotic figures and nuclear sizes (polyploidy) (Figures 1D and S2E–S2H). Flow cytometry analysis further suggested an inflammatory phenotype with an increased proportion of monocytes in OTULIN-deficient livers (Figure S3A–S3D). In addition, this analysis identified a significant proportion of Clec4F^{+}Tim4^{-} Kupffer cells (KCs) in OTULIN^{LPC-KO} livers. Typically, the presence of Tim4^{-} KCs suggests KC death and their subsequent replacement from circulating monocytes, which only gain Tim4 expression with time (Scott et al., 2016; Figures S3A–S3D). The increased expression of pro-inflammatory cytokines and chemokines (*Il6*, *Il1β*, *Rantes*, and *Mcp1*) could also be demonstrated in the OTULIN-deficient liver lysates (Figure 1E). Sirius Red staining, *Tgfb1* mRNA expression, and CK19 immunostaining confirmed the presence of fibrosis, associated with oval cell hyperplasia, in the livers of OTULIN^{LPC-KO} mice (Figures 1F, 1G, and S3E–S3G). Finally, OTULIN-deficient livers showed increased lipid deposition in hepatocytes (Figures 1H and S3H). In contrast to OTULIN^{LPC-KO} mice, liver sections from wild-type mice showed a normal hepatic parenchyma and no signs of inflammation, lipid deposition, or fibrosis (Figures 1D–1H, S2, and S3).

The liver phenotype of OTULIN^{LPC-KO} mice, characterized by chronic inflammation and fibrosis, resembles non-alcoholic steatohepatitis (NASH) in humans and represents a risk factor for the development of HCC (Sherman, 2005). To evaluate

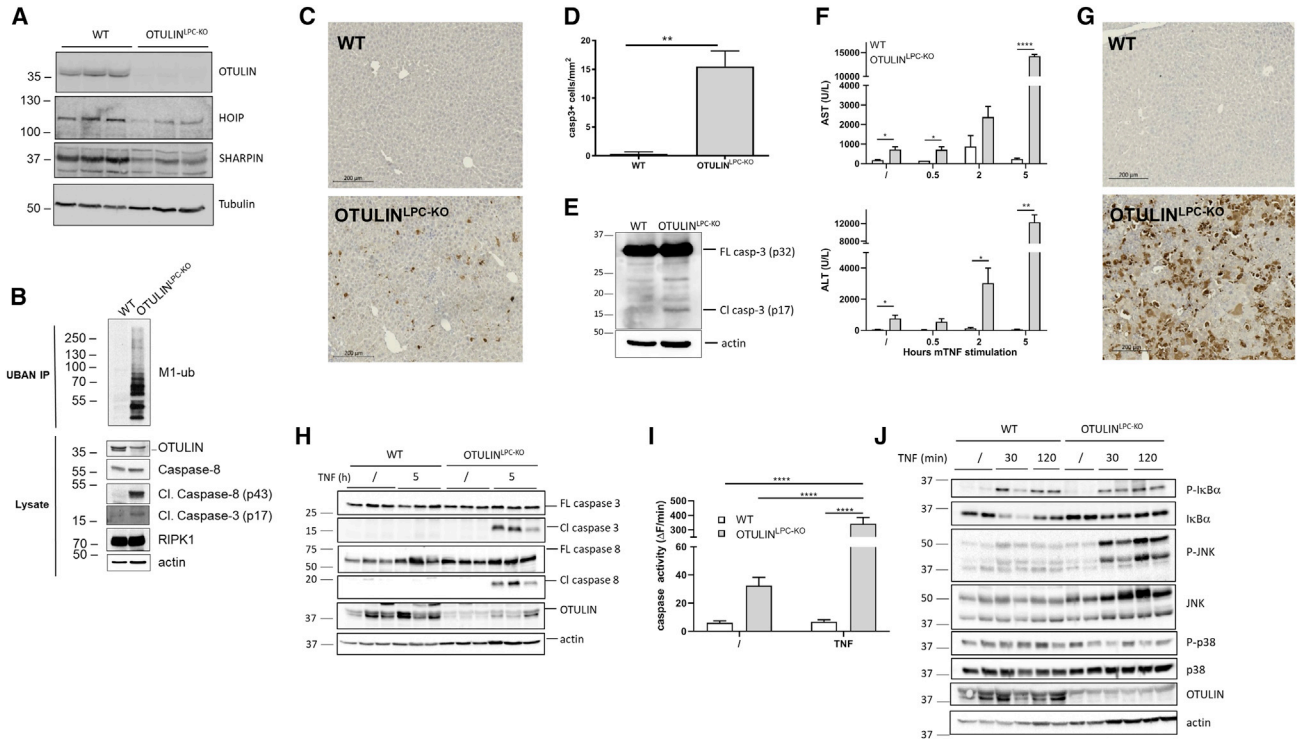

Figure 2. OTULIN Suppresses Linear Ubiquitination and Cell Death in Liver Parenchymal Cells

(A) Western blot analysis for the expression of OTULIN and LUBAC proteins in liver lysates from WT and OTULIN^{LPC-KO} mice. Anti-tubulin immunoblotting was used as a loading control. Data are representative of two independent experiments.

(B) M1 chains were immunoprecipitated from whole liver cell lysates from untreated OTULIN^{LPC-KO} and control littermate mice (WT) using GST-UBANs. Protein levels were determined by immunoblotting. Data are representative of two independent experiments.

(C) Representative images of liver sections from 10-week-old OTULIN^{LPC-KO} and control (WT) mice after immunostaining for cleaved caspase-3. Scale bar, 200 μm.

(D) Quantification of the number of caspase-3^{+} cells. Data are presented as mean ± SEM, n = 5 mice per genotype. **p < 0.01.

(E) Western blot analysis for expression of full-length (FL) and cleaved (Cl) caspase-3 in liver lysates from OTULIN^{LPC-KO} and control littermate mice (WT). Anti-actin immunoblotting was used as a loading control. Data are representative of three independent experiments.

(F) Serum ALT and AST levels of OTULIN^{LPC-KO} (n = 3) and control littermate mice (WT, n = 3) either injected or not injected with 5 μg mouse TNF for the indicated time points. Data are presented as mean ± SEM. *p < 0.05; **p < 0.01; ****p < 0.0001.

(G) Cleaved caspase-3 staining on liver sections from OTULIN^{LPC-KO} mice and control WT littermate mice injected with TNF for 3 h. Scale bar, 200 μm.

(H) Western blot analysis for OTULIN, and FL and Cl caspase-8 and -3 expression in liver lysates from OTULIN^{LPC-KO} and control littermate mice (WT) either injected or not injected with 5 μg mouse TNF for 5 h. Data are representative of two independent experiments.

(I) Caspase activity assayed on liver tissue homogenates of WT (n = 3) and OTULIN^{LPC-KO} littermate (n = 3) mice either injected or not injected with TNF for 5 h. Data are presented as mean ± SEM. ****p < 0.0001. Statistical differences were determined by two-way ANOVA.

(J) Western blot analysis for OTULIN, IκBα, phosphorylated IκBα, JNK, phosphorylated JNK, p38, and phosphorylated p38 in liver lysates from OTULIN^{LPC-KO} and control littermate mice (WT) either injected or not injected with 5 μg mouse TNF for the indicated time points. Anti-actin immunoblotting was used as a loading control. Data are representative of two independent experiments.

whether OTULIN^{LPC-KO} lesions represent pre-neoplastic lesions, which may develop at later stages into HCC, livers from 6-month-old OTULIN^{LPC-KO} mice were dissected. All of the OTULIN^{LPC-KO} mice displayed a severe liver phenotype with the presence of multiple nodules (Figure S4A), which were not detected in the livers of control littermate mice. Histology demonstrated the presence of early well-differentiated HCC in 3 of 8 KO cases (37.5%) (Figure 1I), while the other 5 KO livers displayed diffuse and severe pre-neoplastic lesions reminiscent of HCC. Malignancy was further confirmed in young OTULIN^{LPC-KO} mice by increased RNA levels of several oncofetal HCC marker genes, such as AFP and connective tissue growth factor (CTGF), as well as of hepatic stem cell marker genes, such as glypican 3 (GPC-3) and CD133 (Figures S4B and S4C). By the age of 1 year, all of the OTULIN^{LPC-KO} mice had developed severe liver pathology displaying multiple neoplastic lesions, ranging from adenoma to HCC (Figures S4D–S4G).

OTULIN Deletion Leads to Accumulation of Linear Ubiquitin Chains, but Paradoxically Causes Spontaneous Hepatocyte Apoptosis

LUBAC-mediated linear ubiquitination plays an important role in the activation of the NF-κB signaling pathway and in protecting cells from death (Peltzer et al., 2014, 2018). OTULIN is reported to counteract LUBAC activity by removing the linear chains conjugated to LUBAC substrates, which include TNFR1, NEMO,

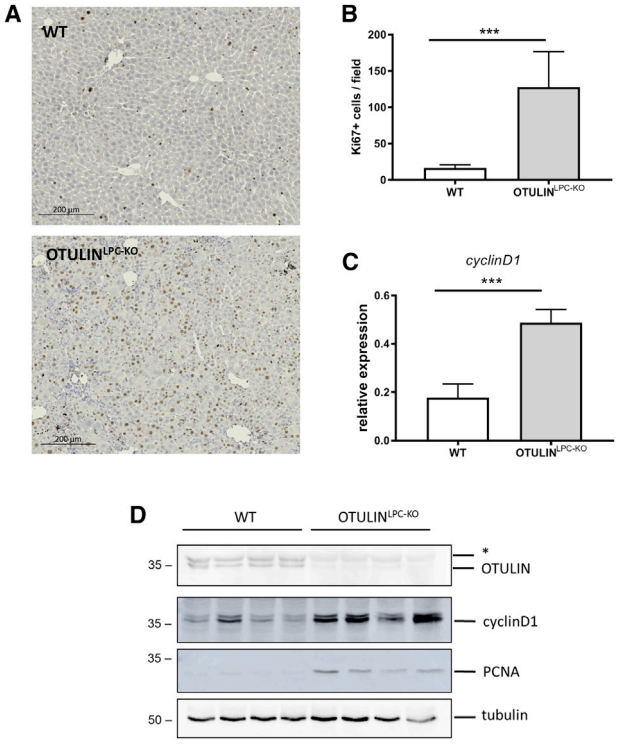

Figure 3. Enhanced Hepatocyte Proliferation in OTULIN-Deficient Livers

(A) Representative images of liver sections from 10-week-old OTULIN^{LPC-KO} mice and control (WT) mice after Ki67 immunostaining for proliferating cells. Scale bar, 200 μm.

(B) Quantification of the number of Ki67^{+} cells. Data are presented as mean ± SEM, n = 5 mice per genotype. ***p < 0.001.

(C) Relative mRNA expression of *Cyclin D1* in total liver lysates from 10-week-old OTULIN^{LPC-KO} mice (n = 12) and control (WT, n = 11) mice. Data are presented as mean ± SEM. ***p < 0.001.

(D) Liver protein extracts from 10-week-old OTULIN^{LPC-KO} mice and control (WT) mice were subjected to western blotting using antibodies detecting OTULIN, cyclin D1, and PCNA. Anti-tubulin immunoblotting was used as a loading control. Data are representative of three independent experiments.

RIPK1, RIPK2, and MyD88 (Hrdinka and Gyrd-Hansen, 2017). In accordance, OTULIN deficiency was shown to cause hyper-ubiquitination of signaling proteins, leading to NF-κB hyper-activation and inflammatory signaling (Hrdinka and Gyrd-Hansen, 2017). A recent report, however, showed that OTULIN promotes rather than counteracts LUBAC activity by preventing its autoubiquitination, and that knockin mice expressing DUB-inactive OTULIN resemble LUBAC-deficient mice and die at midgestation due to pro-inflammatory cell death (Heger et al., 2018). We demonstrated that the specific deletion of OTULIN in hepatocytes resulted in the reduced expression of HOIP and SHARPIN (Figure 2A), as previously reported in other cell types (Heger et al., 2018; Damgaard et al., 2016, 2019), including MEFs (Figure S1A). Despite the reduced LUBAC expression levels, analysis of linear ubiquitination by specific UBAN pulldowns revealed the massive accumulation of linear polyubiquitin in liver lysates of OTULIN-deficient mice (Figure 2B). The accumulation of linear chains caused by OTULIN deletion correlated with increased apoptosis of hepatocytes. In contrast to control livers, OTULIN^{LPC-KO} livers showed dispersed and numerous cleaved caspase-3 and TUNEL^{+} cells, indicative of apoptosis induction (Figures 2C, 2D, S5A, and S5B). The detection of cleaved caspase-8 and -3 in OTULIN-deficient liver lysates further demonstrated that OTULIN deficiency sensitizes hepatocytes to caspase-dependent extrinsic apoptosis (Figures 2B and 2E).

To better understand the role of OTULIN in protecting hepatocytes from apoptosis, we evaluated the consequences of its deficiency in the TNFR1 signaling pathway. For this, OTULIN^{LPC-KO} mice and control littermate mice were injected with a normally sublethal dose of recombinant mouse TNF (5 μg/20 g body weight). In contrast to control mice, which only showed a modest drop in body temperature after injection with TNF, OTULIN^{LPC-KO} mice displayed severe hypothermia (Figure S5C) and high levels of liver-specific AST and ALT enzymes in their serum, indicative of massive liver damage (Figure 2F). OTULIN^{LPC-KO} livers displayed numerous cleaved caspase-3^{+} hepatocytes in response to the TNF challenge (Figure 2G). Hepatocyte apoptosis was further confirmed by the presence of cleaved caspase-8 and -3 in the liver lysates (Figure 2H) and by a caspase-3-specific enzymatic DEVD-activity assay (Figure 2I). Finally, the sensitization to apoptosis was associated with enhanced TNF-induced JNK activation and a slight defect in TNF-induced NF-κB activation, as monitored by reduced IκBα degradation, in OTULIN^{LPC-KO} livers (Figure 2J). Also, *in vitro*, enhanced JNK phosphorylation and reduced NF-κB activation could be observed after TNF stimulation of primary hepatocytes isolated from OTULIN^{LPC-KO} mice (Figure S5D).

These data demonstrate the importance of OTULIN in restricting M1 ubiquitination in hepatocytes and identify OTULIN as an essential protein protecting mice from hepatocyte apoptosis and acute liver failure. These results also demonstrate that despite the spontaneous accumulation of linear polyubiquitin in OTULIN-deficient livers, signaling to NF-κB by TNF is compromised, which may provide a molecular explanation for the spontaneous apoptosis of OTULIN-deficient hepatocytes.

Hepatocyte Apoptosis Is Accompanied by Compensatory Hepatocyte Proliferation in OTULIN-Deficient Livers

The liver has remarkable regenerative capacity, and hepatocytes start massively proliferating following hepatic loss to restore liver function and mass (Luedde et al., 2014). Since hepatocyte apoptosis in OTULIN-deficient mice may be the driving force triggering hepatocyte proliferation favoring hepatocarcinogenesis, we next assessed liver proliferation in OTULIN^{LPC-KO} mice. Hepatocyte apoptosis in OTULIN^{LPC-KO} mice was accompanied by excessive liver cell proliferation, as demonstrated by the increased number of Ki67^{+} cells (Figures 3A and 3B). In agreement, expression of the cell-cycle markers cyclin D1 and proliferating cell nuclear antigen (PCNA) was strongly enhanced in liver lysates of OTULIN^{LPC-KO} mice (Figures 3C and 3D). These data underline the correlation between hepatocyte cell death and proliferation and suggest that the severe liver pathology in OTULIN^{LPC-KO} mice develops as a result of continuous hepatocyte apoptosis and compensatory hepatocyte proliferation,

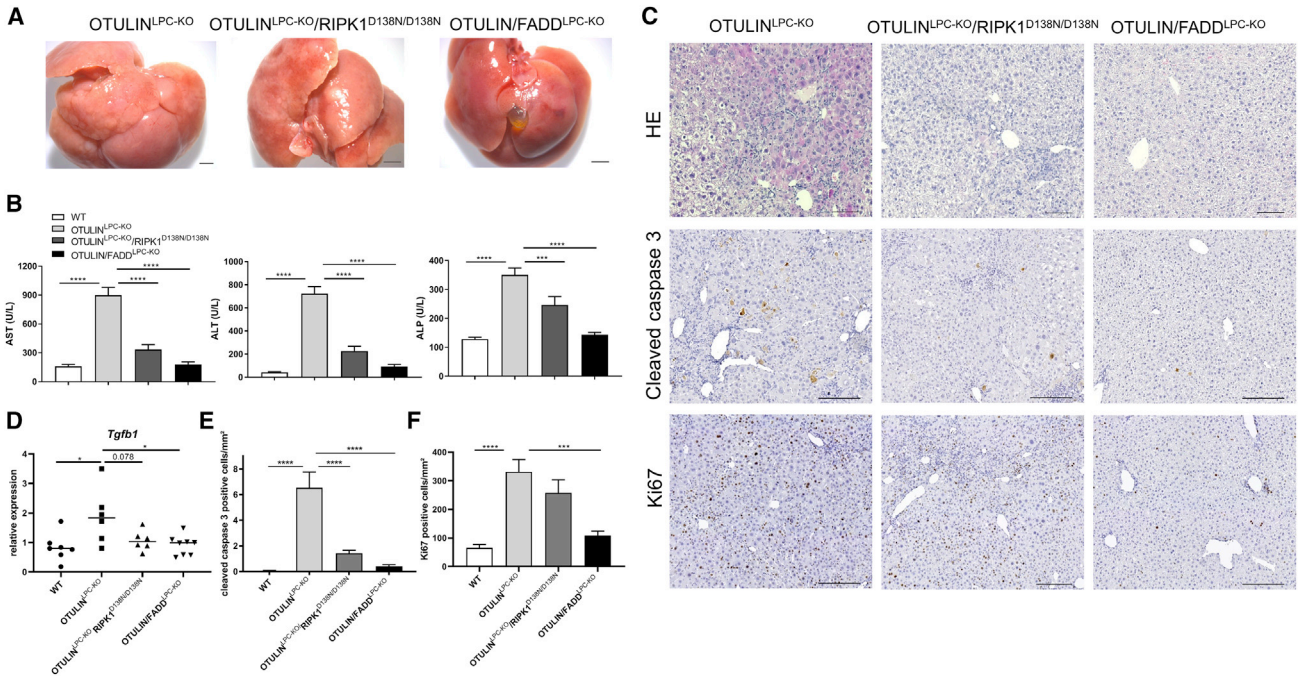

Figure 4. FADD Deficiency or Absence of RIPK1 Kinase Activity Protects OTULIN^{LPC-KO} Mice from Developing Liver Pathology

(A) Macroscopic pictures of representative livers from a 10-week-old OTULIN^{LPC-KO}, OTULIN^{LPC-KO}/RIPK1$^{D138N/D138N}$, and OTULIN/FADD^{LPC-KO} mouse. Scale bar, 2 mm.

(B) Serum ALT, AST, and ALP levels in control (WT, n = 49), OTULIN^{LPC-KO} (n = 22), OTULIN^{LPC-KO}/RIPK1$^{D138N/D138N}$ (n = 11), and OTULIN/FADD^{LPC-KO} (n = 18) mice. Data are presented as mean ± SEM. ***p < 0.001; ****p < 0.0001.

(C) Representative H&E, Cl caspase-3, and Ki67-stained liver section from 10-week-old OTULIN^{LPC-KO}, OTULIN^{LPC-KO}/RIPK1$^{D138N/D138N}$, and OTULIN/FADD^{LPC-KO} mice. Scale bar H&E, 100 μm; cleaved caspase-3 and Ki67, 200 μm.

(D) Relative mRNA expression of *Tgfb1* in total liver lysates from 10-week-old control (WT, n = 7), OTULIN^{LPC-KO} (n = 6), OTULIN^{LPC-KO}/RIPK1$^{D138N/D138N}$ (n = 6), and OTULIN/FADD^{LPC-KO} (n = 8) mice. Data are presented as mean ± SEM. *p < 0.05.

(E) Quantification of the number of cleaved caspase-3^{+} cells in liver sections from control (WT, n = 6), OTULIN^{LPC-KO} (n = 5), OTULIN^{LPC-KO}/RIPK1$^{D138N/D138N}$ (n = 7), and OTULIN/FADD^{LPC-KO} (n = 8) mice. Data are presented as mean ± SEM. ****p < 0.0001.

(F) Quantification of the number of Ki67^{+} cells in liver sections from control (WT, n = 9), OTULIN^{LPC-KO} (n = 6), OTULIN^{LPC-KO}/RIPK1$^{D138N/D138N}$ (n = 8), and OTULIN/FADD^{LPC-KO} (n = 7) mice. Data are presented as mean ± SEM. ***p < 0.001; ****p < 0.0001.

promoting the development of chronic hepatitis, fibrosis, and eventually HCC.

FADD and RIPK1 Kinase Activity-Dependent Apoptosis Drives Hepatocyte Death and Liver Pathology in OTULIN^{LPC-KO} Mice

Since OTULIN was previously shown to be essential to prevent TNF-dependent systemic inflammation in humans and in mice (Zhou et al., 2016; Damgaard et al., 2016, 2019), we next addressed the specific role of TNF in triggering the spontaneous death of OTULIN-deficient hepatocytes, leading to the development of spontaneous liver pathology in OTULIN^{LPC-KO} mice. For this, we generated TNF-deficient OTULIN^{LPC-KO} mice. The genetic deletion of *Tnf* did not prevent spontaneous liver pathology in OTULIN^{LPC-KO} mice (Figure S6A). Although 10-week-old OTULIN^{LPC-KO}/TNF^{KO} mice had lower levels of serum ALT, AST, and ALP compared to the levels seen in OTULIN^{LPC-KO} mice (Figure S6B), histological analysis of liver tissue revealed that the additional deletion of TNF did not significantly reduce immune cell infiltration or the numbers of caspase-3^{+} hepatocytes (Figures S6C–S6E). Similarly, KO of TNFR1 in all of the cells did not protect OTULIN^{LPC-KO} mice from developing liver disease (Figures S6A–S6E). These results demonstrate that TNF signaling does not drive chronic liver damage in OTULIN^{LPC-KO} mice.

Previous studies have demonstrated that the protective role of linear ubiquitination against RIPK1 kinase-dependent and -independent FADD-mediated apoptosis is not limited to TNFR1 signaling (Lafont et al., 2017; Taraborrelli et al., 2018), suggesting conserved regulatory mechanisms downstream of various death receptors. Since RIPK1 has already been implicated in liver pathology by regulating hepatocyte death (Kondylis and Pasparakis, 2019), we evaluated the presence and consequence of RIPK1 kinase-dependent apoptosis of hepatocytes in our OTULIN^{LPC-KO} mice. To do so, we crossed OTULIN^{LPC-KO} mice to knockin mice expressing a kinase-inactive RIPK1-D138N mutant (Polykratis et al., 2014). Ten-week-old OTULIN^{LPC-KO}/RIPK1$^{D138N/D138N}$ mice demonstrated slightly reduced liver pathology, but showed significantly reduced serum ALT, AST, and ALP levels and reduced *Tgfb1* expression compared to OTULIN^{LPC-KO} mice (Figures 4A, 4B, and 4D). Although the livers from OTULIN^{LPC-KO}/RIPK1$^{D138N/D138N}$ mice still revealed aberrant tissue architecture, significantly reduced numbers of

apoptotic hepatocytes but not of proliferating hepatocytes could be observed in the livers from OTULIN^{LPC-KO}/RIPK1$^{D138N/D138N}$ mice compared to OTULIN^{LPC-KO} mice (Figures 4C–4E).

Because RIPK1 kinase activity can induce both FADD-dependent apoptosis and RIPK3/MLKL-dependent necroptosis (Pasparakis and Vandenabeele, 2015), we next evaluated the occurrence of MLKL-dependent hepatocyte necroptosis. OTULIN^{LPC-KO} mice were crossed to mice with a floxed *Mlkl* allele (Murphy et al., 2013), generating mice lacking both OTULIN and MLKL specifically in liver parenchymal cells. MLKL deficiency could, however, not prevent liver pathology in OTULIN^{LPC-KO} mice, as shown by liver histology and detection of liver damage in OTULIN/MLKL^{LPC-KO} mice (Figure S6), arguing against a role for MLKL-driven necroptosis in the OTULIN^{LPC-KO} pathology.

To confirm that hepatocyte apoptosis is responsible for the development of liver pathology in OTULIN^{LPC-KO} mice, we next generated OTULIN^{LPC-KO} mice lacking FADD specifically in liver parenchymal cells by crossing the OTULIN^{LPC-KO} line with mice having a floxed *Fadd* allele (FADD$^{FL/FL}$) (Mc Guire et al., 2010), thereby preventing both RIPK1 kinase-dependent and -independent FADD-mediated apoptosis. In contrast to OTULIN^{LPC-KO} mice, all of which developed severe liver pathology, OTULIN/FADD^{LPC-KO} mice had a completely normal tissue architecture and did not display liver damage, as detected by tissue histology; by serum analysis of ALT, AST, and ALP levels; and by the expression of *Tgfb1* reminiscent of liver fibrosis (Figures 4A–4D). Even in aged 45-week-old mice, no liver pathology could be observed in OTULIN/FADD^{LPC-KO} mice (Figure S7). In agreement, no hepatocyte cell death, shown by cleaved caspase-3 detection in liver tissue sections, could be detected in livers from OTULIN/FADD^{LPC-KO} mice (Figures 4C and 4E). In addition to rescuing hepatocyte death, FADD deficiency inhibited the increased proliferation observed in the livers of OTULIN^{LPC-KO} mice, as shown by the reduced Ki67 staining in liver lysates from OTULIN/FADD^{LPC-KO} mice (Figures 4C and 4F). This demonstrates that the increased hepatocyte proliferation and inflammation in the livers of OTULIN^{LPC-KO} mice are secondary responses to the apoptosis of OTULIN-deficient hepatocytes. These data show that liver disease in OTULIN^{LPC-KO} mice develops as a consequence of FADD-dependent apoptosis, partially driven by RIPK1 kinase activity, but not necroptosis, of OTULIN-deficient hepatocytes.

Finally, since inflammation-induced liver injury is often associated with increased intestinal permeability and bacterial translocation to the liver via the portal vein (Seki and Schnabl, 2012), we assessed the importance of MyD88-dependent signaling for the development of liver pathology in OTULIN^{LPC-KO} mice. Ten-week-old OTULIN^{LPC-KO}/MyD88^{KO} mice were, however, not protected from developing liver disease, and all of them exhibited similar increased serum ALT, AST, and ALP levels compared with OTULIN^{LPC-KO} mice (Figures S6A and S6B). Also, on histology, no differences in immune cell infiltration, hepatocyte cell death, and proliferation could be observed (Figures S6C–S6E).

IFN Signaling Contributes to the Liver Pathology in Hepatocyte-Specific OTULIN KO Mice

The liver phenotype of OTULIN^{LPC-KO} mice was associated with a significant upregulation of inflammatory gene expression, including the expression of IFN response genes, which were reverted to baseline levels in the FADD-deficient genetic background (Figures 1E, 5A, and S8). The serum from OTULIN^{LPC-KO} mice also contained elevated amounts of the IFN-inducible chemokine Cxcl10 (Figure 5B). This suggests that OTULIN may also be important in suppressing the production of type I IFNs, as suggested by recent studies demonstrating the promotion of IFN-α receptor (IFNAR) signaling in conditions in which OTULIN or LUBAC signaling is impaired (Heger et al., 2018; Peltzer et al., 2018). To investigate whether type I IFN signaling contributes to the development of liver pathology in OTULIN^{LPC-KO} mice, we generated OTULIN^{LPC-KO} mice lacking the IFNAR1 (Müller et al., 1994). Ten-week-old OTULIN^{LPC-KO}/IFNAR1^{KO} mice demonstrated reduced liver pathology and showed significantly reduced AST, ALT, and ALP levels compared to OTULIN^{LPC-KO} mice (Figures 5C and 5D). In addition, significantly reduced numbers of apoptotic hepatocytes but not of proliferating hepatocytes could be observed in livers from OTULIN^{LPC-KO}/IFNAR1^{KO} mice compared to those from OTULIN^{LPC-KO} mice (Figures 5E–5G). These data demonstrate that type I IFNs are produced in OTULIN-deficient livers and critically contribute to the severe liver phenotype in OTULIN^{LPC-KO} mice.

DISCUSSION

The incidence of hepatitis and HCC has risen in Western countries, most probably because of changes in dietary habits causing metabolic stress, the metabolic syndrome, and non-alcoholic fatty liver disease (NAFLD). HCC develops as a result of chronic liver inflammation and is mostly diagnosed at advanced stages, with very limited treatment options. Hence, early and sustained suppression of chronic liver damage is key to reducing the risk of developing HCC (Ringelhan et al., 2018). Here, we have demonstrated the spontaneous TNF-independent but FADD-dependent apoptosis of hepatocytes as the crucial event driving liver inflammation, fibrosis, and HCC in hepatocyte-specific OTULIN-deficient mice. Our study also demonstrated that RIPK3-MLKL-dependent hepatocyte necroptosis is not involved in the pathology of OTULIN^{LPC-KO} mice, likely due to the absence of RIPK3 expression in hepatocytes, as previously demonstrated (Dara et al., 2015; Krishna-Subramanian et al., 2019). OTULIN/MLKL^{LPC-KO} mice, lacking both OTULIN and MLKL only in the hepatocytes, seem to display an even worse liver phenotype compared to OTULIN^{LPC-KO} mice. This would suggest that MLKL-dependent necroptosis, eventually through a pathway independent of RIPK3, would protect OTULIN-deficient hepatocytes from death by apoptosis. A recent study demonstrated that the suppression of necroptosis in hepatocytes could promote hepatocyte apoptosis, favoring the development of HCC (Seehawer et al., 2018). This observation suggested that hepatocyte necroptosis generates a liver cytokine microenvironment that promotes the development of intrahepatic cholangiocarcinoma and not HCC from oncogenically transformed hepatic cells (Seehawer et al., 2018). More studies will be needed to investigate this further.

The protective role of LUBAC-mediated linear ubiquitination is well established downstream of TNFR1. On the one hand, it promotes the transcriptional upregulation of anti-apoptotic proteins

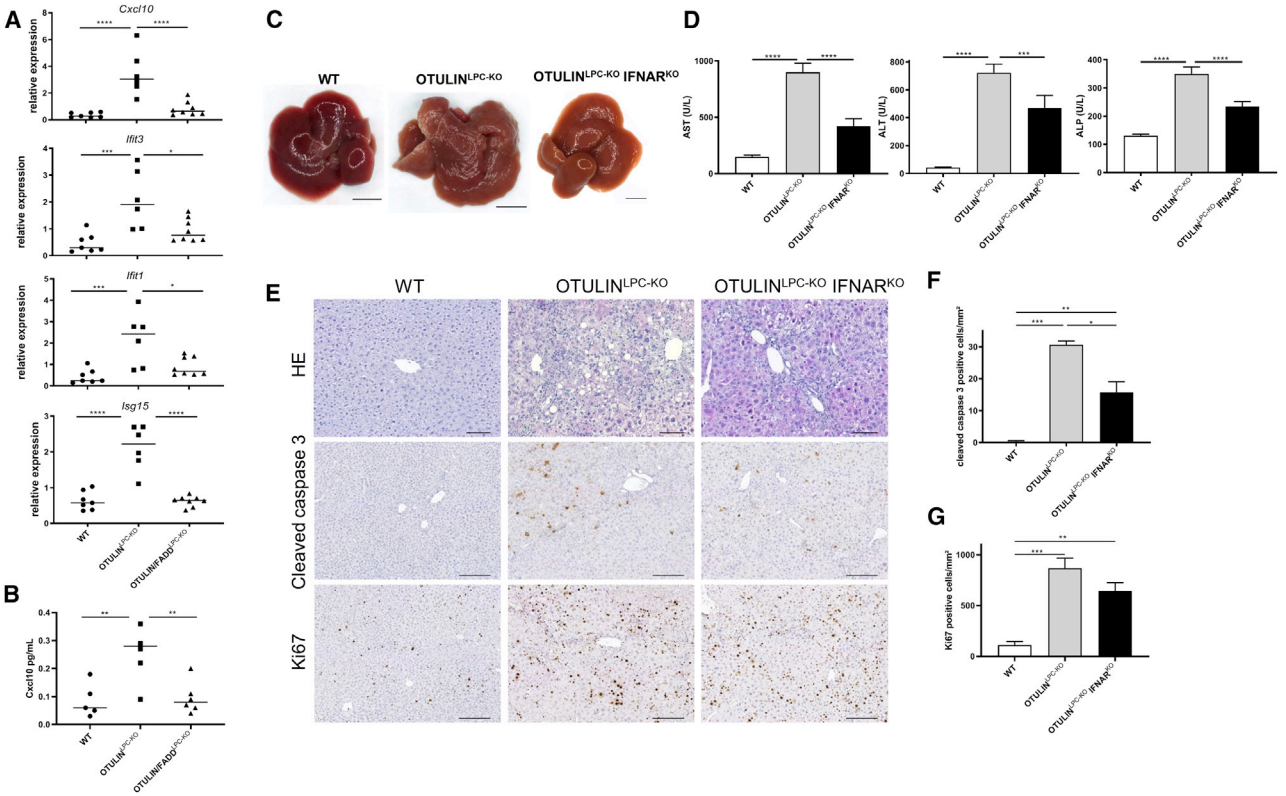

Figure 5. Interferon Signaling Contributes to Liver Pathology in OTULIN^{LPC-KO} Mice

(A) Relative mRNA expression of *Cxcl10*, *Ifit1*, *Ifit3*, and *Isg15* in total liver lysates from 10-week-old control (WT, n = 7), OTULIN^{LPC-KO} (n = 6), and OTULIN/FADD^{LPC-KO} (n = 8) mice. Data are presented as mean ± SEM. *p < 0.05; **p < 0.01; ***p < 0.001; ****p < 0.0001.

(B) Serum Cxcl10 levels in 10-week-old control (WT, n = 5), OTULIN^{LPC-KO} (n = 6), and OTULIN/FADD^{LPC-KO} (n = 6) mice. Data are presented as mean ± SEM. **p < 0.01.

(C) Macroscopic pictures of representative livers from 10-week-old control (WT), OTULIN^{LPC-KO}, and OTULIN^{LPC-KO}/IFNAR1^{KO} mice. Scale bar, 5 mm.

(D) Serum ALT, AST, and ALP levels in control (WT, n = 57), OTULIN^{LPC-KO} (n = 22), and OTULIN^{LPC-KO}/IFNAR1^{KO} (n = 12) mice. Data are presented as mean ± SEM. ***p < 0.001; ****p < 0.0001.

(E) Representative H&E, cleaved caspase-3, and Ki67-stained liver section from 10-week-old control (WT), OTULIN^{LPC-KO}, and OTULIN^{LPC-KO}/IFNAR1^{KO} mice. Scale bar H&E, 100 μm; cleaved caspase-3 and Ki67, 200 μm.

(F) Quantification of the number of Cl caspase-3^{+} cells in liver sections from control (WT, n = 4), OTULIN^{LPC-KO} (n = 3), and OTULIN^{LPC-KO}/IFNAR^{KO} mice (n = 6). Data are presented as mean ± SEM. *p < 0.05; **p < 0.01; ***p < 0.001.

(G) Quantification of the number of Ki67^{+} cells in liver sections from control (WT, n = 4), OTULIN^{LPC-KO} (n = 3), and OTULIN^{LPC-KO}/IFNAR^{KO} mice (n = 6). Data are presented as mean ± SEM. **p < 0.01; ***p < 0.001.

by NF-κB, which protects cells from RIPK1 kinase-independent apoptosis (Wang et al., 2008). On the other hand, it allows the phosphorylation of RIPK1 by IKKα/β and TBK1/IKKε, which was shown to protect cells from RIPK1 kinase-dependent apoptosis (Dondelinger et al., 2015, 2019; Ting and Bertrand, 2016; Lafont et al., 2018; Xu et al., 2018). While several studies have reported the importance of proper TNF signaling for the maintenance of liver homeostasis and to prevent liver inflammation and inflammation-induced HCC (Luedde et al., 2014), our study did not identify TNF as a driving cytokine in the liver pathology of OTULIN^{LPC-KO} mice. The molecular mechanism by which linear ubiquitination protects cells from death may, however, not be limited to TNFR1 but instead be conserved between death receptors. LUBAC was also shown to protect cells from RIPK1 kinase-dependent and -independent FADD-mediated apoptosis downstream of other TNFR superfamily members (Lafont et al., 2017; Taraborrelli et al., 2018). In accordance with this notion, we found that the transgenic expression of a kinase-inactive RIPK1^{D138N} mutant could significantly ameliorate but not fully rescue the liver disease. This indicates that hepatocyte apoptosis in OTULIN^{LPC-KO} mice is FADD/caspase-8 dependent and partially driven by RIPK1 kinase activity. Despite the massive accumulation of linear polyubiquitin, signaling to NF-κB by TNF was compromised in OTULIN-deficient hepatocytes, suggesting that OTULIN deficiency also affects proper signaling to NF-κB downstream of the receptor that triggers apoptosis in OTULIN^{LPC-KO} mice. Therefore, a defect in the NF-κB-mediated upregulation of cytoprotective mechanisms in OTULIN-deficient hepatocytes may account for the RIPK1 kinase-independent hepatocyte apoptosis, while inappropriate regulation of RIPK1 by IKKs may account for the RIPK1 kinase-dependent hepatocyte apoptosis, together inducing liver inflammation and a partial liver pathology.

Since IFNAR1 deficiency protects OTULIN^{LPC-KO} mice, at least partially, from developing severe liver disease, we further demonstrate an important contribution of type I IFNs to the phenotype of OTULIN^{LPC-KO} mice. This observation suggests that OTULIN may also suppress the pathways that are responsible for the production of IFNs, either indirectly by preventing overall inflammation or by direct control of IFN production. In that context, FADD and RIPK1 have been identified as being implicated in an immune defense pathway against intracellular double-stranded RNA (dsRNA) (Balachandran et al., 2004; Michallet et al., 2008; Rajput et al., 2011; Ingram et al., 2019). Further studies are required to identify the pathway(s) regulated by OTULIN driving type I IFN production.

Our results using hepatocyte-specific OTULIN-deficient mice also confirm the importance of linear ubiquitination and its regulation by OTULIN for protection against hepatocyte apoptosis and liver inflammation, which are in agreement with a previous study demonstrating the importance of LUBAC-mediated linear ubiquitination for liver physiology preventing hepatocyte apoptosis, hepatitis, and HCC development (Shimizu et al., 2017).

ORAS (OTULIN-related autoinflammatory syndrome) is a potentially fatal, rare, early-onset autoinflammatory disease caused by homozygous hypomorphic mutations in the human *OTULIN* gene (Zhou et al., 2016; Damgaard et al., 2016, 2019; Nabavi et al., 2019). ORAS patients develop neonatal-onset systemic inflammation, high fevers, dermatitis and panniculitis, diarrhea, and arthritis. However, thus far, no clinical manifestations of liver disease in ORAS patients have been documented nor have *OTULIN* mutations been identified in the livers of HCC patients. Analysis of the TCGA (The Cancer Genome Atlas) microarray dataset (https://www.cancer.gov/about-nci/organization/ccg/research/structural-genomics/tcga) indicated an increase rather than a decrease in *OTULIN* mRNA levels in HCC tissues (n = 374) compared with normal liver tissue (n = 50) (p = 5.91e−12 comparing all tumor samples; p = 3.55e−6 comparing 50 paired tumor samples). While these results are intriguing, it remains unknown whether OTULIN expression in these liver samples is relevant for HCC or simply a consequence of liver pathology.

In conclusion, with our studies, we identified OTULIN as a critical regulator of liver homeostasis by protecting the liver parenchymal cells from death by apoptosis, which could drive liver inflammation, fibrosis, and eventually liver cancer, similar to what has been demonstrated for NEMO (Luedde et al., 2007; Kondylis et al., 2015). Blockade of hepatocyte cell death may thus have therapeutic potential for patients suffering from chronic inflammatory liver diseases. Also, hepatocyte-specific OTULIN-deficient mice may serve as a novel model to study NAFLD and HCC and help to develop new treatments for the diagnosis of or therapeutic intervention in patients suffering from inflammation-induced liver pathologies risking the development of HCC.

STAR★METHODS

Detailed methods are provided in the online version of this paper and include the following:

- KEY RESOURCES TABLE
- LEAD CONTACT AND MATERIALS AVAILABILITY
- EXPERIMENTAL MODEL AND SUBJECT DETAILS
  - Animals
  - Cells
- METHOD DETAILS
  - Mice
  - Generation of hepatocyte-specific OTULIN knockout mice
  - Isolation and immortalization of mouse embryonic fibroblasts (MEFs)
  - Isolation of liver cells for immune profiling
  - Primary hepatocytes
  - Western blot analysis
  - Immunoprecipitation
  - Cell death assay
  - Liver injury
  - Histology
  - Histological scoring
  - Cxcl10 detection
  - Quantitative real-time PCR
  - TCGA database analysis
- QUANTIFICATION AND STATISTICAL ANALYSIS
- DATA AND CODE AVAILABILITY

SUPPLEMENTAL INFORMATION

Supplemental Information can be found online at https://doi.org/10.1016/j.celrep.2020.01.028.

ACKNOWLEDGMENTS

We thank the European Conditional Mouse Mutagenesis Program (EUCOMM) consortium for *Otulin*-targeted embryonic stem cells (ESCs). We thank Alexander Warren and James Murphy (The Walter and Eliza Hall Institute of Medical Research, Melbourne, Australia) for the use of floxed *Mlkl* mice. We are grateful to Laetitia Bellen for animal care. L.V. is a predoctoral fellow supported by a doctoral scholarship from the Special Research Fund of the Ghent University and by a Research Foundation Flanders (FWO) doctoral fellowship, and A.M. is a predoctoral fellow supported by a grant from the Concerted Research Actions (GOA, BOF14/GOA/013) of Ghent University. Research in the van Loo lab is supported by VIB and research grants from the FWO, the Geneeskundige Stichting Koningin Elisabeth (GSKE), the CBC Banque Prize, the European Charcot Foundation, the Belgian Foundation against Cancer (FAF-F/2018/1200), and Kom op tegen Kanker.

AUTHOR CONTRIBUTIONS

L.V., A.M., D.P., M.S., H.V., L.V.H., S.V., L.B., and C.L.S. performed the experiments. L.V., E.H., C.L.S., J.R., J.M., A.d.B., Y.S., M.J.M.B., and G.v.L. analyzed the data. M.P. provided the mice. G.v.L. provided ideas and coordinated the project. L.V. and G.v.L. wrote the manuscript.

DECLARATION OF INTERESTS

The authors declare no competing interests.

Received: September 26, 2019
Revised: December 16, 2019
Accepted: January 8, 2020
Published: February 18, 2020

REFERENCES

Adachi, O., Kawai, T., Takeda, K., Matsumoto, M., Tsutsui, H., Sakagami, M., Nakanishi, K., and Akira, S. (1998). Targeted disruption of the MyD88 gene results in loss of IL-1- and IL-18-mediated function. Immunity *9*, 143–150.

Balachandran, S., Thomas, E., and Barber, G.N. (2004). A FADD-dependent innate immune mechanism in mammalian cells. Nature *432*, 401–405.

Bonnardel, J., T'Jonck, W., Gaublomme, D., Browaeys, R., Scott, C.L., Martens, L., Vanneste, B., De Prijck, S., Nedospasov, S.A., Kremer, A., et al. (2019). Stellate Cells, Hepatocytes, and Endothelial Cells Imprint the Kupffer Cell Identity on Monocytes Colonizing the Liver Macrophage Niche. Immunity *51*, 638–654.e9.

Clark, K., Peggie, M., Plater, L., Sorcek, R.J., Young, E.R.R., Madwed, J.B., Hough, J., McIver, E.G., and Cohen, P. (2011). Novel cross-talk within the IKK family controls innate immunity. Biochem. J. *434*, 93–104.

Damgaard, R.B., Walker, J.A., Marco-Casanova, P., Morgan, N.V., Titheradge, H.L., Elliott, P.R., McHale, D., Maher, E.R., McKenzie, A.N.J., and Komander, D. (2016). The Deubiquitinase OTULIN Is an Essential Negative Regulator of Inflammation and Autoimmunity. Cell *166*, 1215–1230.e20.

Damgaard, R.B., Elliott, P.R., Swatek, K.N., Maher, E.R., Stepensky, P., Elpeleg, O., Komander, D., and Berkun, Y. (2019). OTULIN deficiency in ORAS causes cell type-specific LUBAC degradation, dysregulated TNF signalling and cell death. EMBO Mol. Med. *11*, e9324.

Dara, L., Johnson, H., Suda, J., Win, S., Gaarde, W., Han, D., and Kaplowitz, N. (2015). Receptor interacting protein kinase 1 mediates murine acetaminophen toxicity independent of the necrosome and not through necroptosis. Hepatology *62*, 1847–1857.

Dondelinger, Y., Jouan-Lanhouet, S., Divert, T., Theatre, E., Bertin, J., Gough, P.J., Giansanti, P., Heck, A.J.R., Dejardin, E., Vandenabeele, P., and Bertrand, M.J. (2015). NF-κB-Independent Role of IKKα/IKKβ in Preventing RIPK1 Kinase-Dependent Apoptotic and Necroptotic Cell Death during TNF Signaling. Mol. Cell *60*, 63–76.

Dondelinger, Y., Delanghe, T., Priem, D., Wynosky-Dolfi, M.A., Sorobetea, D., Rojas-Rivera, D., Giansanti, P., Roelandt, R., Gropengiesser, J., Ruckdeschel, K., et al. (2019). Serine 25 phosphorylation inhibits RIPK1 kinase-dependent cell death in models of infection and inflammation. Nat. Commun. *10*, 1729.

Heger, K., Wickliffe, K.E., Ndoja, A., Zhang, J., Murthy, A., Dugger, D.L., Maltzman, A., de Sousa E Melo, F., Hung, J., Zeng, Y., et al. (2018). OTULIN limits cell death and inflammation by deubiquitinating LUBAC. Nature *559*, 120–124.

Hrdinka, M., and Gyrd-Hansen, M. (2017). The Met1-Linked Ubiquitin Machinery: Emerging Themes of (De)regulation. Mol. Cell *68*, 265–280.

Hübscher, S.G. (2006). Histological assessment of non-alcoholic fatty liver disease. Histopathology *49*, 450–465.

Ingram, J.P., Thapa, R.J., Fisher, A., Tummers, B., Zhang, T., Yin, C., Rodriguez, D.A., Guo, H., Lane, R., Williams, R., et al. (2019). ZBP1/DAI Drives RIPK3-Mediated Cell Death Induced by IFNs in the Absence of RIPK1. J. Immunol. *203*, 1348–1355.

Iwai, K., Fujita, H., and Sasaki, Y. (2014). Linear ubiquitin chains: NF-κB signalling, cell death and beyond. Nat. Rev. Mol. Cell Biol. *15*, 503–508.

Kellendonk, C., Opherk, C., Anlag, K., Schütz, G., and Tronche, F. (2000). Hepatocyte-specific expression of Cre recombinase. Genesis *26*, 151–153.

Keusekotten, K., Elliott, P.R., Glockner, L., Fiil, B.K., Damgaard, R.B., Kulathu, Y., Wauer, T., Hospenthal, M.K., Gyrd-Hansen, M., Krappmann, D., et al. (2013). OTULIN antagonizes LUBAC signaling by specifically hydrolyzing Met1-linked polyubiquitin. Cell *153*, 1312–1326.

Kleiner, D.E., Brunt, E.M., Van Natta, M., Behling, C., Contos, M.J., Cummings, O.W., Ferrell, L.D., Liu, Y.-C., Torbenson, M.S., Unalp-Arida, A., et al.; Nonalcoholic Steatohepatitis Clinical Research Network (2005). Design and validation of a histological scoring system for nonalcoholic fatty liver disease. Hepatology *41*, 1313–1321.

Kondo, F. (2009). Histological features of early hepatocellular carcinomas and their developmental process: for daily practical clinical application: hepatocellular carcinoma. Hepatol. Int. *3*, 283–293.

Kondylis, V., and Pasparakis, M. (2019). RIP Kinases in Liver Cell Death, Inflammation and Cancer. Trends Mol. Med. *25*, 47–63.

Kondylis, V., Polykratis, A., Ehlken, H., Ochoa-Callejero, L., Straub, B.K., Krishna-Subramanian, S., Van, T.-M., Curth, H.-M., Heise, N., Weih, F., et al. (2015). NEMO Prevents Steatohepatitis and Hepatocellular Carcinoma by Inhibiting RIPK1 Kinase Activity-Mediated Hepatocyte Apoptosis. Cancer Cell *28*, 582–598.

Krishna-Subramanian, S., Singer, S., Armaka, M., Banales, J.M., Holzer, K., Schirmacher, P., Walczak, H., Kollias, G., Pasparakis, M., and Kondylis, V. (2019). RIPK1 and death receptor signaling drive biliary damage and early liver tumorigenesis in mice with chronic hepatobiliary injury. Cell Death Differ. *26*, 2710–2726.

Lafont, E., Kantari-Mimoun, C., Draber, P., De Miguel, D., Hartwig, T., Reichert, M., Kupka, S., Shimizu, Y., Taraborrelli, L., Spit, M., et al. (2017). The linear ubiquitin chain assembly complex regulates TRAIL-induced gene activation and cell death. EMBO J. *36*, 1147–1166.

Lafont, E., Draber, P., Rieser, E., Reichert, M., Kupka, S., de Miguel, D., Draberova, H., von Mässenhausen, A., Bhamra, A., Henderson, S., et al. (2018). TBK1 and IKKε prevent TNF-induced cell death by RIPK1 phosphorylation. Nat. Cell Biol. *20*, 1389–1399.

Luedde, T., and Schwabe, R.F. (2011). NF-κB in the liver–linking injury, fibrosis and hepatocellular carcinoma. Nat. Rev. Gastroenterol. Hepatol. *8*, 108–118.

Luedde, T., Beraza, N., Kotsikoris, V., van Loo, G., Nenci, A., De Vos, R., Roskams, T., Trautwein, C., and Pasparakis, M. (2007). Deletion of NEMO/IKKgamma in liver parenchymal cells causes steatohepatitis and hepatocellular carcinoma. Cancer Cell *11*, 119–132.

Luedde, T., Kaplowitz, N., and Schwabe, R.F. (2014). Cell death and cell death responses in liver disease: mechanisms and clinical relevance. Gastroenterology *147*, 765–783.e4.

Mc Guire, C., Volckaert, T., Wolke, U., Sze, M., de Rycke, R., Waisman, A., Prinz, M., Beyaert, R., Pasparakis, M., and van Loo, G. (2010). Oligodendrocyte-specific FADD deletion protects mice from autoimmune-mediated demyelination. J. Immunol. *185*, 7646–7653.

Mederacke, I., Dapito, D.H., Affò, S., Uchinami, H., and Schwabe, R.F. (2015). High-yield and high-purity isolation of hepatic stellate cells from normal and fibrotic mouse livers. Nat. Protoc. *10*, 305–315.

Michallet, M.-C., Meylan, E., Ermolaeva, M.A., Vazquez, J., Rebsamen, M., Curran, J., Poeck, H., Bscheider, M., Hartmann, G., König, M., et al. (2008). TRADD protein is an essential component of the RIG-like helicase antiviral pathway. Immunity *28*, 651–661.

Müller, U., Steinhoff, U., Reis, L.F., Hemmi, S., Pavlovic, J., Zinkernagel, R.M., and Aguet, M. (1994). Functional role of type I and type II interferons in antiviral defense. Science *264*, 1918–1921.

Murphy, J.M., Czabotar, P.E., Hildebrand, J.M., Lucet, I.S., Zhang, J.-G., Alvarez-Diaz, S., Lewis, R., Lalaoui, N., Metcalf, D., Webb, A.I., et al. (2013). The pseudokinase MLKL mediates necroptosis via a molecular switch mechanism. Immunity *39*, 443–453.

Nabavi, M., Shahrooei, M., Rokni-Zadeh, H., Vrancken, J., Changi-Ashtiani, M., Darabi, K., Manian, M., Seif, F., Meyts, I., Voet, A., et al. (2019). Autoinflammation in a Patient with a Novel Homozygous OTULIN Mutation. J. Clin. Immunol. *39*, 138–141.

Park, Y.N. (2011). Update on precursor and early lesions of hepatocellular carcinomas. Arch. Pathol. Lab. Med. *135*, 704–715.

Pasparakis, M., and Vandenabeele, P. (2015). Necroptosis and its role in inflammation. Nature *517*, 311–320.

Pasparakis, M., Alexopoulou, L., Episkopou, V., and Kollias, G. (1996). Immune and inflammatory responses in TNF alpha-deficient mice: a critical requirement for TNF alpha in the formation of primary B cell follicles, follicular dendritic cell networks and germinal centers, and in the maturation of the humoral immune response. J. Exp. Med. *184*, 1397–1411.

Peltzer, N., Rieser, E., Taraborrelli, L., Draber, P., Darding, M., Pernaute, B., Shimizu, Y., Sarr, A., Draberova, H., Montinaro, A., et al. (2014). HOIP

deficiency causes embryonic lethality by aberrant TNFR1-mediated endothelial cell death. Cell Rep. *9*, 153–165.

Peltzer, N., Darding, M., Montinaro, A., Draber, P., Draberova, H., Kupka, S., Rieser, E., Fisher, A., Hutchinson, C., Taraborrelli, L., et al. (2018). LUBAC is essential for embryogenesis by preventing cell death and enabling haematopoiesis. Nature *557*, 112–117.

Pfeffer, K., Matsuyama, T., Kündig, T.M., Wakeham, A., Kishihara, K., Shahinian, A., Wiegmann, K., Ohashi, P.S., Krönke, M., and Mak, T.W. (1993). Mice deficient for the 55 kd tumor necrosis factor receptor are resistant to endotoxic shock, yet succumb to L. monocytogenes infection. Cell *73*, 457–467.

Polykratis, A., Hermance, N., Zelic, M., Roderick, J., Kim, C., Van, T.-M., Lee, T.H., Chan, F.K.M., Pasparakis, M., and Kelliher, M.A. (2014). Cutting edge: RIPK1 Kinase inactive mice are viable and protected from TNF-induced necroptosis in vivo. J. Immunol. *193*, 1539–1543.

Priem, D., Devos, M., Druwé, S., Martens, A., Slowicka, K., Ting, A.T., Pasparakis, M., Declercq, W., Vandenabeele, P., van Loo, G., and Bertrand, M.J.M. (2019). A20 protects cells from TNF-induced apoptosis through linear ubiquitin-dependent and -independent mechanisms. Cell Death Dis. *10*, 692.

Rajput, A., Kovalenko, A., Bogdanov, K., Yang, S.-H., Kang, T.-B., Kim, J.-C., Du, J., and Wallach, D. (2011). RIG-I RNA helicase activation of IRF3 transcription factor is negatively regulated by caspase-8-mediated cleavage of the RIP1 protein. Immunity *34*, 340–351.

Ringelhan, M., Pfister, D., O'Connor, T., Pikarsky, E., and Heikenwalder, M. (2018). The immunology of hepatocellular carcinoma. Nat. Immunol. *19*, 222–232.

Rivkin, E., Almeida, S.M., Ceccarelli, D.F., Juang, Y.-C., MacLean, T.A., Srikumar, T., Huang, H., Dunham, W.H., Fukumura, R., Xie, G., et al. (2013). The linear ubiquitin-specific deubiquitinase gumby regulates angiogenesis. Nature *498*, 318–324.

Rodríguez, C.I., Buchholz, F., Galloway, J., Sequerra, R., Kasper, J., Ayala, R., Stewart, A.F., and Dymecki, S.M. (2000). High-efficiency deleter mice show that FLPe is an alternative to Cre-loxP. Nat. Genet. *25*, 139–140.

Schlageter, M., Terracciano, L.M., D'Angelo, S., and Sorrentino, P. (2014). Histopathology of hepatocellular carcinoma. World J. Gastroenterol. *20*, 15955–15964.

Scott, C.L., Zheng, F., De Baetselier, P., Martens, L., Saeys, Y., De Prijck, S., Lippens, S., Abels, C., Schoonooghe, S., Raes, G., et al. (2016). Bone marrow-derived monocytes give rise to self-renewing and fully differentiated Kupffer cells. Nat. Commun. *7*, 10321.

Seehawer, M., Heinzmann, F., D'Artista, L., Harbig, J., Roux, P.-F., Hoenicke, L., Dang, H., Klotz, S., Robinson, L., Doré, G., et al. (2018). Necroptosis microenvironment directs lineage commitment in liver cancer. Nature *562*, 69–75.

Seki, E., and Schnabl, B. (2012). Role of innate immunity and the microbiota in liver fibrosis: crosstalk between the liver and gut. J. Physiol. *590*, 447–458.

Sherman, M. (2005). Hepatocellular carcinoma: epidemiology, risk factors, and screening. Semin. Liver Dis. *25*, 143–154.

Shimizu, Y., Peltzer, N., Sevko, A., Lafont, E., Sarr, A., Draberova, H., and Walczak, H. (2017). The Linear ubiquitin chain assembly complex acts as a liver tumor suppressor and inhibits hepatocyte apoptosis and hepatitis. Hepatology *65*, 1963–1978.

Taraborrelli, L., Peltzer, N., Montinaro, A., Kupka, S., Rieser, E., Hartwig, T., Sarr, A., Darding, M., Draber, P., Haas, T.L., et al. (2018). LUBAC prevents lethal dermatitis by inhibiting cell death induced by TNF, TRAIL and CD95L. Nat. Commun. *9*, 3910.

Thoolen, B., Maronpot, R.R., Harada, T., Nyska, A., Rousseaux, C., Nolte, T., Malarkey, D.E., Kaufmann, W., Küttler, K., Deschl, U., et al. (2010). Proliferative and nonproliferative lesions of the rat and mouse hepatobiliary system. Toxicol. Pathol. *38* (*7 Suppl*), 5S–81S.

Ting, A.T., and Bertrand, M.J.M. (2016). More to Life than NF-κB in TNFR1 Signaling. Trends Immunol. *37*, 535–545.

Wang, L., Du, F., and Wang, X. (2008). TNF-α induces two distinct caspase-8 activation pathways. Cell *133*, 693–703.

Xu, D., Jin, T., Zhu, H., Chen, H., Ofengeim, D., Zou, C., Mifflin, L., Pan, L., Amin, P., Li, W., et al. (2018). TBK1 Suppresses RIPK1-Driven Apoptosis and Inflammation during Development and in Aging. Cell *174*, 1477–1491.e19.

Zhou, Q., Yu, X., Demirkaya, E., Deuitch, N., Stone, D., Tsai, W.L., Kuehn, H.S., Wang, H., Yang, D., Park, Y.H., et al. (2016). Biallelic hypomorphic mutations in a linear deubiquitinase define otulipenia, an early-onset autoinflammatory disease. Proc. Natl. Acad. Sci. USA *113*, 10127–10132.

STAR★METHODS

KEY RESOURCES TABLE

REAGENT or RESOURCE	SOURCE	IDENTIFIER
Antibodies		
cleaved caspase 3	Cell Signaling Technology	Cat# 9661; RRID:AB_2341188
Ki67	Cell Signaling Technology	Cat# 12202; RRID:AB_2620142
goat anti-rabbit	Agilent	Cat# E0432; RRID:AB_2313609
Otulin	Cell Signaling Technology	Cat# 14127; RRID:AB_2576213
A20	Santa Cruz Biotechnology	Cat# sc-166692; RRID:AB_2204516
caspase 3	Cell Signaling Technology	Cat# 9662; RRID:AB_331439
JNK	BD Bioscience	Cat# 554285; RRID:AB_395344
P-JNK	Millipore	Cat# PS1019-100UL; RRID:AB_10696844
IkBa	Santa Cruz Biotechnology	Cat# sc-371; RRID:AB_2235952
P-IkBa	Cell Signaling Technology	Cat# 9246; RRID:AB_2267145
Sharpin	Proteintech	Cat# 14626-1-AP; RRID:AB_2187734
Cyclin D1	Abcam	Cat# ab190564
Tubulin	Sigma-Aldrich	Cat# T4026; RRID:AB_477577
PCNA	Novus	Cat# NB500-106; RRID:AB_2252058
b-actin	Santa Cruz Biotechnology	Cat# sc-47778 HRP; RRID:AB_2714189
anti-rabbit-IgG-HRP	GE Healthcare	Cat# GENA934; RRID:AB_2722659
anti-mouse-IgG-HRP	GE Healthcare	Cat# NA931; RRID:AB_772210
anti-goat-IgG-HRP	Santa Cruz Biotechnology	Cat# sc-2354; RRID:AB_628490
CD26-FITC	BD Biosciences	Cat# 559652; RRID:AB_397295
CD172a-BB630P	BD Bioscience	custom conjugate
Tim4-Percp-eFluor710	Thermo Fisher Scientific	Cat# 46-5866-82; RRID:AB_2573781
Clec4F-unconjugated	R and D Systems	Cat# AF2784; RRID:AB_2081339
Goat IgG-AF647	Thermo Fisher Scientific	Cat# A-21447; RRID:AB_2535864
Live/dead dye – APCeFluor780	eBioscience	cat#65-0865-18
Ly6C-eFluor450	Thermo Fisher Scientific	Cat# 48-5932-82; RRID:AB_10805519
CD45-BV510	BioLegend	Cat# 103138; RRID:AB_2563061
CD11b-BV605	BD Biosciences	Cat# 563015; RRID:AB_2737951
CD64-BV711	BioLegend	Cat# 139311; RRID:AB_256384
F4/80-BV786	BioLegend	Cat# 123141; RRID:AB_2563667
XCR1-BV650	BioLegend	Cat# 148220; RRID:AB_2566410
SiglecF-BUV395	BD Biosciences	Cat# 740280; RRID:AB_2740019
Ly6G-BUV563	BD Biosciences	cat#612921
MHCII-BUV805	BD Biosciences	custom conjugate
CD11c-PE-eFluor610	Thermo Fisher Scientific	Cat# 61-0114-82; RRID:AB_2574530
CD3	Tonbo Biosciences	Cat# 70-0031; RRID:AB_2621472
CD19	Thermo Fisher Scientific	Cat# 35-0193-82; RRID:AB_891395
B220	BD Biosciences	Cat# 553091; RRID:AB_394621
NK1.1-PE-Cy5	BioLegend	Cat# 108716; RRID:AB_493590
Ripk1	Cell Signaling Technology	Cat# 3493; RRID:AB_2305314
cleaved caspase 8	Cell Signaling Technology	Cat# 9429; RRID:AB_2068300
caspase 8	Abnova Corporation	Cat# MAB3429; RRID:AB_10629060
Anti-Linear Ubiquitin Antibody, clone LUB9	Millipore	cat#MABS451
goat anti-rabbit polyclonal IgG biotin	Agilent	cat# E043201; RRID:AB_2313609

(*Continued on next page*)

Continued

REAGENT or RESOURCE	SOURCE	IDENTIFIER
CK19	Lammer lab	n/a
hoip	Damgaard lab	n/a
hoil-1	Walczak lab	n/a
Chemicals, Peptides, and Recombinant Proteins		
TRIzol reagent	Thermo Fisher Scientific	cat#15596026
mTNF	This paper	n/a
Collagenase A	Sigma-Aldrich	cat#11088793001
GST-UBAN	Ivan Dikic lab	n/a
DNase	Roche	cat#04 536 282 001
DMEM	GIBCO	cat# 41965-062
DMEM F12	GIBCO	cat# 31330-038
non essential aminoacids	Lonza	cat#BE13-114E
L-glutamin	Lonza	cat# BE17-605F
bovine collagen 1	Nutacon	n/a
Sodium pyruvate	Sigma-Aldrich	cat# S-8636
Penicillin-Streptomycin	GIBCO	cat#15140-122
fetal calf serum	Bodinco	n/a
Complete, EDTA-free Protease Inhibitor Cocktail Tablets	Roche	cat#11873580001
PhosStop	Roche	cat# 04906837001
Antigen retrieval buffer	Dako	cat# S-203130
hydrogen peroxide 30%	Sigma-Aldrich	cat# H-1009
Hematoxylin Mayer's	Sigma	cat# 51275-500ml
Entellan	Merck	cat# 107961
Neg −50 Kryo-Medium	Thermo Fisher Scientific	cat# 6506
Direct Red 80	Sigma	cat# 365548
Ac-DEVD-MCA	PeptaNova	cat# 3171-V
Critical Commercial Assays		
Aurum Total RNA Isolation Mini Kit	BioRad	cat# 7326820
Sensifast cDNA Synthesis Kit	Bioline	cat#BIO-65054
SensiFAST SYBR® No-ROX Kit	GeC Biotech	cat# CSA-01190
Vectastain ELITE ABC Kit Standard	Vector Laboratories	cat# PK-6100
ImmPACT DAB Peroxidase (HRP) Substrate	Vector Laboratories	cat# SK-4105
Western Lightning Plus ECL	Perkin Elmer	cat# NEL101001EA
TUNEL	Millipore	cat#17-141
Trygliceride colorimetric assay kit	Cayman chemical	cat#10010303
Deposited Data		
TCGA database	n/a	https://www.cancer.gov/about-nci/organization/ccg/research/structural-genomics/tcga
Experimental Models: Cell Lines		
mouse: primary hepatocytes	this paper	n/a
OTULIN^{KO} MEFs	this paper	n/a
Experimental Models: Organisms/Strains		
mouse: OTULIN^{FL}	this paper	n/a
mouse: Alfp Cre	Kellendonk et al., 2000	n/a
mouse: Mlkl^{FL}	Murphy et al., 2013	n/a
mouse: Fadd^{FL}	Mc Guire al., 2010	n/a
mouse: Ripk1^{D138N}	Polykratis et al., 2014	n/a

(*Continued on next page*)

Continued		
REAGENT or RESOURCE	SOURCE	IDENTIFIER
mouse: MyD88$^{-/-}$	Adachi et al., 1998	n/a
mouse: Tnf$^{-/-}$	Pasparakis et al., 1996	n/a
mouse: Tnfr1$^{-/-}$	Pfeffer et al., 1993	n/a
mouse: Ifnar$^{-/-}$	Müller et al., 1994	n/a
Oligonucleotides		
qPCR primers see Table S1	n/a	n/a
Software and Algorithms		
ZEN (blue edition)	Zeiss	https://www.zeiss.com/microscopy/int/products/microscope-software/zen.html
FlowJo.10	n/a	https://www.flowjo.com/
GraphPad Prism 8	n/a	https://www.graphpad.com/
Fluostar Omega	BMG Labtech	https://www.bmglabtech.com/fluostar-omega/
Other		
Axioscan	Zeiss	n/a
BDSymphony	BD Biosciences	n/a
LightCycler 480 II	Roche	n/a
Amersham Imager 600	GE Healthcare	n/a

LEAD CONTACT AND MATERIALS AVAILABILITY

Further information and requests for resources and reagents may be directed to Geert van Loo (Lead Contact; geert.vanloo@irc.vib-ugent.be). Resources and reagents generated in this study are available from the Lead Contact but may require a Materials Transfer Agreement to be signed.

EXPERIMENTAL MODEL AND SUBJECT DETAILS

Animals

The following mouse lines were used: Alfp-Cre (Kellendonk et al., 2000), *Fadd*^{FL} (Mc Guire al., 2010), *Mlkl*^{FL} (Murphy et al., 2013), *Ripk1*^{D138N} (Polykratis et al., 2014), *Myd88*$^{-/-}$ (Adachi et al., 1998), *Tnf*$^{-/-}$ (Pasparakis et al., 1996), *Tnfr1*$^{-/-}$ (Pfeffer et al., 1993) and *Ifnar1*$^{-/-}$ (Müller et al., 1994). *Otulin* floxed mice were generated from *Otulin/Fam105btm1a* C57BL/6 embryonic stem (ES) cells (generated by the European Mouse Mutagenesis (EUCOMM) Programme). All experiments on mice were conducted according to institutional, national and European animal regulations. Animal protocols were approved by the ethics committee of Ghent University. Mice were housed in individually ventilated cages at the VIB Center for Inflammation Research, in a specific pathogen-free animal facility. Mice were housed in temperature- and humidity-controlled conditions at 21°C and 60% relative humidity, 14/10 h light/darkness. Further, a wooden stick and nesting material (tissues) were present as environmental enrichment. Food and regular drinking water were provided *ad libitum* for all experiments. All experiments were performed on 10-52-week old mice. All mice had a C57BL/6 genetic background. Both sexes were used in this study and littermates were used as controls in all experiments.

Cells

MEFs were grown in complete DMEM (DMEM (GIBCO) medium supplemented with 10% fetal calf serum (Bodinco), 1% penicillin/streptomycin (GIBCO), 1% L-Glutamine (Lonza), 0.4% sodium-pyruvate (Sigma) and 1% non-essential amino acids (Lonza)). MEFs were grown at 37°C, 5% CO_2 and 5% O_2. The sex of the MEFs cells was never determined as these cells were isolated from embryos. Primary hepatocytes were grown on plates coated with collagen (Nutacon) in DMEM F12 (GIBCO) supplemented with 10% fetal calf serum (Bodinco) and 1% penicillin/streptomycin (GIBCO). Primary hepatocytes were grown at 37°C and 5% CO_2. Primary hepatocytes were isolated both from male and female mice.

METHOD DETAILS

Mice

The following mouse lines were used: Alfp-Cre (Kellendonk et al., 2000), *Fadd*^{FL} (Mc Guire al., 2010), *Mlkl*^{FL} (Murphy et al., 2013), *Ripk1*^{D138N} (Polykratis et al., 2014), *Myd88*$^{-/-}$ (Adachi et al., 1998), *Tnf*$^{-/-}$ (Pasparakis et al., 1996), *Tnfr1*$^{-/-}$ (Pfeffer et al., 1993)

and *Ifnar1*$^{-/-}$ (Müller et al., 1994). All alleles were maintained on a C57BL/6 genetic background. Mice were housed in individually ventilated cages at the VIB Center for Inflammation Research, in a specific pathogen-free animal facility. All experiments on mice were conducted according to institutional, national and European animal regulations. Animal protocols were approved by the ethics committee of Ghent University.

Generation of hepatocyte-specific OTULIN knockout mice

C57BL/6 embryonic stem (ES) cells with an *Otulin/Fam105b*^{tm1a} allele were generated by the European Mouse Mutagenesis (EUCOMM) Programme using a 'knockout-first with conditional potential' gene targeting cassette, and used to generate mice bearing a neomycin-LacZ cassette and a loxP-flanked exon 3 of *Otulin*. For this, the targeted ES cell clone was injected into 3.5-day blastocysts and transferred to the uteri of pseudopregnant foster mothers. Male chimeras were mated with C57BL/6 females to obtain germline transmission of the *Otulin* floxed allele (still containing the neomycine selection cassette, *Otulin*^{NFL}). The Frt-flanked neomycin-LacZ cassette was removed by crossing *Otulin*^{NFL} mice with a Flp-deleter strain (Rodríguez et al., 2000) generating an *Otulin* floxed allele (*Otulin*^{FL}). *Otulin*$^{FL/FL}$ mice were crossed to Alfp-Cre transgenic mice (Kellendonk et al., 2000) to generate liver parenchymal cell-specific OTULIN knockout (*Otulin*$^{LPC\text{-}KO}$) mice (Figure S1C, D).

Isolation and immortalization of mouse embryonic fibroblasts (MEFs)

Otulin$^{+/-}$ mice were generated by crossing chimeras transmitting the *Otulin*^{FL} genotype with Cre-deleter mice. MEFs were prepared from E10.5 Otulin$^{+/+}$, Otulin$^{+/-}$ and Otulin$^{-/-}$ embryos, and immortalized through serial passaging and frozen in liquid nitrogen.

Isolation of liver cells for immune profiling

The protocol for the isolation of liver cells was adapted from Mederacke et al. (2015) as previously described (Bonnardel et al., 2019). Briefly, after retrograde cannulation, livers were first perfused with an EGTA-containing solution for 1–2 min following by a perfusion with 0.2 mg/ml collagenase A-containing solution for 5 min (6 ml/min). Livers were minced and incubated for 20 min with 0.4 mg/ml Collagenase A and 10 U/ml DNase in a water bath at 37°C. All subsequent procedures were performed at 4°C. After filtration with a 100 μm mesh filter, the cell suspensions were centrifuged at 400 g for 7 min and re-suspended in 2 mL of red blood lysis buffer for 3 min. Suspensions were washed in PBS and further filtered on a 40 μm mesh filter and centrifuged twice for 1 min at 50 g resulting in an hepatocytes-enriched fraction (pellet) and a leukocytes/LSECs/HSCs-enriched fraction (supernatant). Both fractions were further centrifuged at 400 g for 7 min before proceeding with FACS staining. After staining cells were analyzed on a BDSymphony and resulting data were analyzed using FlowJo Software. Following antibodies were used: CD26-FITC (BD, Cat no: 559652), CD172a-BB630P (BD, Custom conjugate), Tim4-Percp-eFluor710 (Thermo Fischer, Cat no: 46-5866-82), Clec4F-unconjugated (R&D systems, Cat no: AF2784), Goat IgG-AF647 (Thermo Fischer, Cat no: A-21447), Fixable Live/dead dye – APCeFluor780, Ly6C-eFluor450 (eBioscience – Cat no: 48-5932-82), CD45-BV510 (Biolegend, Cat no: 103138), CD11b-BV605 (BD, Cat no: 563015), CD64-BV711 (Biolegend, Cat no: 139311), F4/80-BV786 (Biolegend, Cat no: 123141), XCR1-BV650 (Biolegend, Cat no: 148220), SiglecF-BUV395 (BD, Cat no: 740280), Ly6G-BUV563 (BD, Cat no: 612921), MHCII-BUV805 (BD, custom conjugate), CD11c-PE-eFluor610 (eBioscience, Cat no: 61-0114-82), Lineage markers – CD3 (TONB55-0031-U100, Tonbo Biosciences), CD19 (15-1093-83, eBioscience), B220 (553091, BD), NK1.1-PE-Cy5 (108716, Biolegend).

Primary hepatocytes

Hepatocytes were isolated as described above (*Isolation of liver cells for immune profiling*). Cells were seeded and cultured in DMEM F12 with 10% fetal calf serum (Bodinco) and 1% penicillin/streptomycin (GIBCO). Cells were left untreated or stimulated with mTNF (20 ng/mL, VIB Protein Service Facility) for the indicated time points.

Western blot analysis

Cells and liver tissue were homogenized using E1A lysis buffer (50 mM HEPES pH7.6; 250 mM NaCl; 5 mM EDTA; 0.5% NP40) and RIPA (50 mM Tris-HCl, pH 7.6; 1 mM EDTA; 150 mM NaCl; 1% NP-40; 0.5% sodiumdeoxycholate; 0.1% SDS) buffer respectively containing protease inhibitors (Roche) and phosphatase inhibitors (Sigma), denaturated in 1 x Laemmli buffer (50 mM Tris-HCl pH8.2; 2% SDS; 10% glycerol; 0.005% BFB; 5% β-mercapto-ethanol) and boiled for 10 min at 95°C. 50 μg of liver lysates and 20 ug of cell lysates were separated by SDS-polyacrylamide gel electrophoresis (PAGE), transferred to nitrocellulose and analyzed by immunoblotting. Membranes were probed with antibodies against OTULIN (1:1000, Cell Signaling Technology), A20 (1:1000, Santa Cruz Biotechnologies), caspase-3 (full length and cleaved) (1:1000, Cell Signaling Technology), cleaved caspase-8 (1:1000, Cell Signaling Technology), caspase-8 (1:1000, Abnova), JNK (1:1000, BD Bioscience), phospho-JNK (1:1000, Sigma-Aldrich), IκBα (1:1000, Santa Cruz Biotechnologies), phospho-IκBα (1:1000, Cell Signaling Technology), HOIL-1 (1:2000, kind gift of Dr. Henning Walczak, UCL London), HOIP (1:1000, kind gift of Dr. Rune Damgaard, MRC Cambridge), Sharpin (1:1000, Proteintech, 1:1000), PCNA (1:1000, Novus), cyclin-D1 (1:1000, Abcam), Ripk1 (1:2000, Cell Signaling Technology), linear ubiquitin (1:2500, Millipore), tubulin (1: 1000, Sigma-Aldrich) and actin-HRP (1:10000, MP Biomedicals). As secondary antibodies, HRP coupled anti-rabbit-HRP, anti-mouse-HRP and anti-goat-HRP were used (1:2500, Amersham) and detection was done by chemiluminescence (Western Lightning Plus ECL, Perkin Elmer) using the Amersham Imager 600 (GE Healthcare).

Immunoprecipitation

Recombinant GST-UBAN was produced in BL21(DE3) cells. In brief, BL21(DE3) cells were transformed with the plasmid encoding GST-UBAN and protein expression was induced with 0.5 M IPTG. After 4 h, cells were collected and lysed in lysis buffer (20 mM Tris-HCl pH 7.5, 10 mM EDTA, 5mM EGTA, 150 mM NaCl, 1mM DTT supplemented with phosphatase and protease inhibitor cocktail tablets (Roche Diagnostics)), sonicated and cleared by centrifugation. After centrifugation, Triton X-100 (0.5% final concentration) was added to the supernatant, which was then transferred onto prewashed glutathione beads and left rotating for 2 h at 4°C. After incubation, the beads were centrifuged, washed twice with washing buffer (20 mM Tris-HCl pH 7.5, 10 mM EDTA, 150 mM NaCl, 0.5% Triton X-100) and resuspended in resuspension buffer (20 mM Tris-HCl pH 7.5, 0.1% β-mercaptoethanol, 0.05% sodiumazide), ready to be used. Cell lysates from total liver tissue were prepared as described before, protein concentration was determined and 5 mg protein lysate was incubated overnight with GST-UBAN-containing glutathione beads. The next day, the beads were washed three times in RIPA lysis buffer (150 mM NaCl, 1% NP-40, 0.5% Sodium Deoxycholate, 0.1% SDS, 10 mM Tris-HCl pH 8 supplemented with phosphatase and protease inhibitor cocktail tablets (Roche Diagnostics)). Beads were then resuspended in 60 μL 1x laemmli buffer for direct analysis.

Cell death assay

Liver tissues were lysed in caspase lysis buffer (1% NP-40, 200 mM NaCl, 10 mM Tris-HCl pH 7, 5 mM EDTA, 10% glycerol, freshly supplemented with Complete, EDTA-free Protease Inhibitor Cocktail Tablets (Roche)) and volume was adjusted to reach a protein concentration of 2 μg/μl. 20 μg of cell lysate was added to 140 μl of CFS buffer (10 mM HEPES pH 7.5, 220 mM mannitol, 68 mM sucrose, 2 mM NaCl, 2 mM MgCl2, 2.5 mM KH2PO4, supplemented with 10 mM DTT and Complete, EDTA-free Protease Inhibitor Cocktail Tablets (Roche)) containing 50 μM acetyl-Asp-Glu-Val-Asp-aminomethylcoumarin (Ac-DEVD-amc, PeptaNova). Caspase-3 activation was measured at intervals of 3 min using a Fluostar Omega fluorescence plate reader, with an excitation filter of 360 nm, an emission filter of 460 nm, gains set at 900, 10 flashes per well and orbital averaging with a diameter of 3 mm.

Liver injury

Mice were injected i.p. with a sublethal dose of mouse TNF (5 μg mouse TNF/20 g body weight). *E. coli*-derived recombinant mTNF had a specific activity of 9.46 × 107 IU/mg, and was produced and purified to homogeneity in our laboratory with endotoxin levels not exceeding 1 ng/mg protein. Mice were euthanized after 2.5 h for histological analysis. Serum alkaline phosphatase (ALP), alanine transaminase (ALT), aspartate transaminase (AST) and bilirubin levels were measured in the Laboratory of Clinical Biology of the University Hospital Gent, according to standard procedures.

Histology

Livers were dissected and fixed in 4% paraformaldehyde and embedded in paraffin. Sections were stained with Hematoxylin/Eosin (HE) or with specific stains or antibodies. For immunohistochemistry, following dewaxing, slides were incubated in antigen retrieval solution (Dako), boiled for 20 min in a PickCell cooking unit and cooled down for 3 h. Endogenous peroxidase activity was blocked by incubating the slides in 3% wv H_2O_2 (Sigma). The blocking buffer contains 0.2% goat serum, 0.5% Fish skin gelatin and 2% BSA in PBS. Subsequently slides were incubated with primary antibodies overnight at 4°C: anti-cleaved caspase 3 (1:300, Cell Signaling), anti-Ki67 (1:1000, Cell Signaling) or rabbit anti-CK19 (1:600, kindly provided by Wout Lamers, AMC, Amsterdam). Next, the slides were incubated with biotin coupled goat anti-rabbit (1:500, Dako). Subsequently, slides were incubated in ABC solution (Vectastain ELITE ABC Kit Standard, Vector Laboratories). Peroxidase activity was detected by adding diaminobutyric acid (DAB) substrate (ImmPACT DAB Peroxidase (HRP) Substrate, Vector Laboratories), and slides were counterstained with hematoxylin (Sigma), dehydrated and mounted with Entellan (Merck). TUNEL kit (Millipore) was used to visualize apoptotic cells, according to manufacturer's instructions. The pictures were taken with the Zeiss slide scanner. For Sirus red staining, slides were dried overnight at 55°C, nuclei were stained with Weigert's hematoxylin (Sigma) and then slides were incubated with Sirius red solution, made by 0,5 g Sirius Red (Direct Red 80, Sigma) and 500 mL saturated aqueous solution of picric acid (1.3% in water, Sigma). For Oil Red O staining, liver samples were fixed in 4% PFA for 2 h and incubated in 30% sucrose overnight after which they were frozen in OCT cryostat embedding medium (Neg −50 Kryo-Medium, Thermo Fisher Scientific). Coupes were fixed in 4% PFA and subsequently incubated in 100% propylene glycol, Oil Red O (at 60°C) and 85% propylene glycol. The sections were counterstained with hematoxylin (Sigma).

Histological scoring

Histological diagnosis was performed on HE-stained slides using standard histopathological analysis based on cellular morphology of mouse liver lesions (Thoolen et al., 2010). The main lesions observed were classified and eventually scored (0: none/minimal; 1: mild; 2:moderate; 3: severe) as: foci of necrosis, portal, and lobular inflammation/immune cells infiltration, anisocytosis, and anisokaryosis (respectively, variations of cellular and nuclear size and shape), pigmented macrophages, intranuclear pseudoinclusions, foci of vacuolar changes, lobular dysplasia, hepatocellular hypertrophy, foci of cellular alteration (FCA), adenoma, hepatocellular carcinoma (HCC). Oval cell proliferation was evaluated based on a grading system applied to stage precirrhotic/cirrhotic lesions in mouse liver (Kleiner et al., 2005; Hübscher, 2006) as following: STAGE 1: perisinusoidal or periportal (1A: mild, zone3, perinusoidal; 1B: moderate, zone 3, perisinusoidal; 1C: portal/periportal only); STAGE 2: perisinusoidal and portal/periportal; STAGE 3: bridging fibrosis/oval cell proliferation; STAGE 4: cirrhosis. The number of mitotic figures and apoptotic cells was evaluated in 5 randomly

selected HPF (high power fields, 40X). Differentiation between dysplastic nodules (DNs) and early HCC was based on criteria published for the analysis of human liver (Kondo, 2009; Park, 2011; Schlageter et al., 2014). Due to the difficulty in distinguishing early HCC from DNs in some of the liver samples, a further category indicated with ''indiscernible'' nodular lesion has been introduced, characterized by a transitional histological appearance in between the two lesions. The immunohistochemistry for Ki67 and CK19 was also evaluated in order to distinguish between these two lesions. The following criteria have been applied to analyze the nodules: 1) higher cellularity (usually 2 times that of the surrounding hepatic parenchyma in HCC); 2) plate thickness and/or pseudoglandular (microacinar) structures (typical of HCC); 3) stromal invasion: well differentiated tumor cells invade the fibrous tissue of portal tracts with lack of ductular reaction (evident by the analysis of CK19 stained slides, typical of HCC); 4) presence of portal tracts (evident by CK19 IHC, present in varying number, usually reduced in HCC; may be present in HNs and DNs); 5) higher number of Ki67-positive hepatocytes (evaluated by IHC, compared to the surrounding parenchyma); 6) vacuolar changes (common in HCC, may be present in DNs); 7) lack of distinct demarcation (more typical of HCC); 8) cellular pleomorphism and loss of normal lobular architecture (present in both DNs and HCC); 9) compression (typical of adenoma when compression of adjacent normal hepatocytes is seen at least on two quadrants). Ki67, Caspase 3 and TUNEL stained slides were evaluated under a microscope, counting the number of positive nuclei in ten randomly selected high power fields, 40X. The total number of positive nuclei for each was divided by 10 to obtain the index. Positive cells within inflammatory foci and areas of oval cell hyperplasia/fibrosis were excluded from the count. The extent of the hepatic parenchyma stained with CK19 and Sirius red was evaluated by semiquantitative grading (0: none/minimal; 1: mild; 2: moderate; 3: severe).

Cxcl10 detection

Serum was isolated from adult mice and Cxcl10 was measured by Bio-Plex (Biorad, Pro Mouse Chemokine IP-10/CXCL10 Set), according to manufacturer's instructions.

Quantitative real-time PCR

Total RNA was isolated using TRIzol reagent (Invitrogen) and Aurum Total RNA Isolation Mini Kit (Biorad), according to manufacturer's instructions. Synthesis of cDNA was performed using Sensifast cDNA Synthesis Kit (Bioline) according to the manufacturer's instructions. cDNA was amplified on quantitative PCR in a total volume of 5 μl with SensiFAST SYBR® No-ROX Kit (Bioline) and specific primers on a LightCycler 480 (Roche). The reactions were performed in triplicates. Mouse-specific primers that were used for this study can be found in Table S1, related to STAR Methods.

TCGA database analysis

Liver cancer gene expression profiles in the TCGA database (https://www.cancer.gov/about-nci/organization/ccg/research/structural-genomics/tcga) were downloaded using the R package TCGA-assembler, including 424 HCC and liver samples of mRNA expression profiles. Gene expression values were plotted as log2(CPM) values.

QUANTIFICATION AND STATISTICAL ANALYSIS

Results are expressed as the mean ± SEM, with n the number of mice. Normality tests (Kolmogorov-Smirnov) were performed to check for normal distribution of the data. As all data were normally distribute, parametric tests were performed to check the statistical significance between different groups. Statistical significance between WT and $OTULIN^{LPC-KO}$ was assessed using an unpaired two-sample Student t-Test, unless stated otherwise. Statistical significance between $OTULIN^{LPC-KO}$ and the different genetic crosses was assessed using a one-way ANOVA test, followed by Tukey's multiple comparison test. The analysis was performed with Prism software (V8). Statistical details can be found in the figure legends.

DATA AND CODE AVAILABILITY

This study did not generate datasets or code.